

Nonparametric Control-Koopman Operator Learning: Flexible and Scalable Models for Prediction and Control*

Petar Bevanda[†], Bas Driessen[‡], Lucian Cristian Iacob[‡], Roland Tóth^{‡§}, Stefan Sosnowski[†], and Sandra Hirche[†]

Abstract. Linearity of Koopman operators and simplicity of their estimators coupled with model-reduction capabilities has led to their great popularity in applications for learning dynamical systems. While nonparametric Koopman operator learning in infinite-dimensional reproducing kernel Hilbert spaces is well understood for autonomous systems, its control system analogues are largely unexplored. Addressing systems with control inputs in a principled manner is crucial for fully data-driven learning of controllers, especially since existing approaches commonly resort to representational heuristics or parametric models of limited expressiveness and scalability. We address the aforementioned challenge by proposing a universal framework via *control-affine reproducing kernels* that enables direct estimation of a single operator even for control systems. The proposed approach, called *control-Koopman operator regression* (cKOR), is thus completely analogous to Koopman operator regression of the autonomous case. First in the literature, we present a nonparametric framework for learning Koopman operator representations of nonlinear control-affine systems that does not suffer from the curse of control input dimensionality. This allows for reformulating the infinite-dimensional learning problem in a finite-dimensional space based solely on data without apriori loss of precision due to a restriction to a finite span of functions or inputs as in other approaches. For enabling applications to large-scale control systems, we also enhance the scalability of control-Koopman operator estimators by leveraging random projections (sketching). The efficacy of our novel cKOR approach is demonstrated on both forecasting and control tasks.

Key words. Koopman operators, kernel methods, control systems, reproducing kernel Hilbert spaces, vector-valued regression, machine learning

MSC codes. 47N70, 47B32, 47B33, 37N35

1. Introduction. In recent years, there is an ever-growing interest across different fields in constructing operator-theoretic models that can provide *global* insight into physical or biological characteristics of observed phenomena [28], e.g., in terms of facilitating tractable analysis and control design for nonlinear dynamics [10, 14, 73, 15]. While, historically, physical insight based on *first principles* was the driving force in modeling, increasing system complexity [63, 61] limits their utility for modeling in engineering, necessitating the use of data-driven methods. A promising framework that has recently reemerged and has gained traction in the data-driven modeling community is based on the Koopman operator [48], whose spectral decomposition can enable linear superposition of signals for possibly highly nonlinear systems

*Last updated: May 14, 2024.

Funding: This work received financial support of the EU Horizon 2020 research and innovation programme “SeaClear” under grant agreement no. 871295.

[†]Chair of Information-oriented Control (ITR), TUM School of Computation, Information and Technology, Technical University of Munich, Munich, Germany (petar.bevanda@tum.de, sosnowski@tum.de, hirche@tum.de).

[‡]Control Systems Group, Eindhoven University of Technology, Eindhoven, The Netherlands (b.j.l.driessen@student.tue.nl, l.c.iacob@tue.nl, r.toth@tue.nl).

[§]Systems and Control Laboratory, HUN-REN Institute for Computer Science and Control, Budapest, Hungary.

[15]. This representational simplicity of dynamics inspired a bevy of applications from system identification [57, 72, 3, 74], soft robotics [12, 36], optimal control [90, 34, 40], optimization algorithms [25, 26] to analysing long-term [46, 96] and multiscale dynamics [31, 23, 7, 30].

Koopman-based representation theory for control systems. As the Koopman framework was originally developed for autonomous systems, to accommodate control inputs, different methods have been proposed. These range from heuristically selecting a fully linear model class [51], having a finite set of input values and describing a switched model [76] or analytically deriving the lifted representation [32]. It has become established that control-affine systems can be written as bilinear lifted models under certain conditions, at least in continuous time. The authors of [42] show that for both continuous and discrete-time systems with inputs, an invariant Koopman form can be analytically derived, granted that the autonomous part can be exactly embedded. The resulting model class contains a state and input-dependent input contribution, which is often not bilinear, especially in the discrete-time case. Thus, a globally exact finite-dimensional representation generally requires a non-affine nonlinear control effect or a recasting to a *linear parameter-varying* (LPV) model form. While this has been shown on an analytic level for finite dimensional Koopman operator-based representations, it is an open question if nonlinear input terms are unavoidable in the infinite-dimensional case and if a possible approximation error could be controlled in a data-driven setting.

Data-driven Koopman approaches for control. Though a number of deep learning-enhanced, yet parametric, methods [35, 37, 8] have been proposed, their theoretical analysis is often limited to existence, i.e., density/universal approximation results. For example, showing existence of a network of given size achieving a certain error rate, does not provide guarantees whether this network is computable in practice. To alleviate these issues, kernel-based operator learning provides a powerful alternative [4] that is mathematically and implementation-wise simple, but offers rigorously established avenues for *a priori* error analysis and convergence theory. Unsurprisingly, the aforementioned lead to the recent increase in the learning-theoretic understanding of nonparametric Koopman operator-based models for dynamical systems [9, 54, 53]. Nevertheless, their control system counterparts lag behind and do not enjoy a comparable level of understanding – lacking rigorously established operator estimators that can handle large system classes, learning using arbitrary control-input data while working in, flexible, infinite-dimensional spaces. The reason for the aforementioned is primarily rooted in an early discretization of the learning problem, e.g., by an explicit and fixed feature or input dependence [80, 78, 44, 68, 69], which commonly leads to a systematic loss of precision and inefficient exploitation of the data [45]. Such prior restriction to a data-independent finite-dimensional subspace is especially ill-suited when dealing with unknown large-scale systems that require a suitably large/rich feature or input space. As summarized in Table 1, existing data-driven operator-theoretic control system models do not enable control and autonomous effects to be jointly infinite-dimensional and require multiple operator regressions. Additionally, many approaches require multiple datasets (cf. Table 1), e.g., additional constant input datasets, to approximate the corresponding Koopman generators and have an irreducible error at forecasting due to Euler discretization. Such restrictions commonly exclude most data-driven settings, e.g., learning from a dataset, ensuring sufficient exploration or safe data collection.

We alleviate these issues of parametric methods with a holistic approach by proposing an end-to-end use of the *reproducing property* – “kernel trick” [39] – through a control-affine

Table 1: Comparison with existing operator learning approaches for control systems. The notions of state and control domains are that of their sampling operators in RKHS, and $|\cdot|$ denotes cardinality. The support for various empirical risk minimization (ERM) estimators, scalability and the inherent utilization of infinite dimensions highlights the *flexibility* of our *cKOR* approach.

Approach	input samples	control domain	state domain	datasets	ERM	scalability
switched \mathbf{u} [75]	quantized	finite	finite	$n_{\mathbf{u}}+1$	✗	✗
bEDMD: [13, 71];	arbitrary	finite	finite	1	✗	✓ ¹
[76, 83, 69]/[77] ²	constant	finite	finite / ∞	$n_{\mathbf{u}}+1$	✗	✗
cKOR (ours)	arbitrary	∞	∞	1	✓	✓

kernel. The former turns out to be crucial in getting a hold on both the approximation error and high-dimensional feature and control spaces, avoiding the explicit tensor products of dictionary and control inputs [71, 87]. As our experiments confirm, this property leads to superior performance of our nonparametric approach over classically used parametric approaches, approximating highly accurate Galerkin methods from data [51, 98]. Crucially, our framework does not need commonly unavailable derivative information, approximate interpolation of different fixed-input Koopman operators or multiple regressions found in existing works [75, 69, 77]. We address these issues simultaneously by a novel nonparametric operator learning method, providing a natural control-affine counterpart to statistical learning approaches for autonomous dynamics [54, 59].

1.1. Contributions.

- Prove that discrete-time control-affine systems admit universal infinite-dimensional bilinear state-space models.
- Propose nonparametric control-Koopman operators expressing many operator-based control system representations from the literature as particular cases.
- Derive data-driven estimators for control-Koopman operators, expressing state-space models in a closed form.
- Derive the sketched/Nyström counterparts to the KRR estimator for scalable learning.
- Demonstrate the compatibility of classical POD techniques on our operator-based control system models for additional model order reduction.

1.2. Notation. For non-negative integers n and m , $[m, n] = \{m, m+1, \dots, n\}$ with $n \geq m$ gives an interval set of integers, and define $[n] := [1, n]$. Given two separable Hilbert spaces \mathcal{H} and \mathcal{G} , we let $\text{HS}(\mathcal{H}, \mathcal{G})$ be a Hilbert space of Hilbert-Schmidt (HS) operators from \mathcal{H} to \mathcal{G} endowed with the norm $\|A\|_{\text{HS}}^2 \equiv \sum_{i \in \mathbb{N}} \|Ae_i\|_{\mathcal{G}}^2$, for $\text{HS}(\mathcal{H}, \mathcal{G})$ where $\{e_i\}_{i \in \mathbb{N}}$ is an orthonormal basis of \mathcal{H} . When using (Koopman) composition operators, different time steps are related as $\mathcal{A}_{t+s} = \mathcal{A}_s \mathcal{A}_t$ and when omitting time-step subscripts we assume $t = 1$. For simplicity, with a slight abuse of notation, adjoint of operators as well as conjugate transposes of a

¹Limited by a tensor product of inputs and features.

²Lacking infinite-dimensional covariance operators modeling control-affine dependencies due to interpolating estimated Koopman operators for $n_{\mathbf{u}} + 1$ constant inputs.

matrices are denoted as $(\cdot)^\top$. Lower/upper case symbols denote functions/operators while bold symbols reserved for matrices and vectors. The space of square-integrable functions is denoted as $L^2(\cdot)$ with an appropriate Lebesgue measure while the vector space of continuous functions is denoted by $\mathcal{C}(\cdot)$. We let $k : \mathbb{X} \times \mathbb{X} \rightarrow \mathbb{R}$ be a symmetric and positive definite kernel function and \mathcal{H} the corresponding RKHS [43], with norm denoted as $\|\cdot\|_{\mathcal{H}}$. For $\mathbf{x} \in \mathbb{X}$, we use $\mathbf{x} \mapsto k_{\mathbf{x}} \equiv k(\cdot, \mathbf{x}) \in \mathcal{H}$ to denote the canonical feature map. We differentiate between input-steered RKHS and its autonomous analogue using $\mathcal{H}_U, \mathcal{H}_X$, respectively.

2. Problem statement. Consider an unknown nonlinear control affine system given by

$$(2.1) \quad \mathbf{x}_{t+1} := \mathbf{f}(\mathbf{x}_t) + \sum_{j=1}^{n_u} \mathbf{g}_j(\mathbf{x}_t) u_j(t) \equiv \mathbf{f}_o(\mathbf{x}_t, \mathbf{u}_t)$$

where $\mathbf{x}_t \equiv \mathbf{x}(t) \in \mathbb{X} \subseteq \mathbb{R}^{n_x}$ is the state variable and $\mathbf{u}_t := [u_1(t) \cdots u_{n_u}(t)]^\top \in \mathbb{U} \subseteq \mathbb{R}^{n_u}$ denotes the input variable and $t \in \mathbb{Z}_0^+$ is the discrete time. Control-affinity in (2.1) is often sufficient to represent the dynamical behaviour of many engineering applications [60]. Additionally, more general representation of nonlinear systems characterized by unstructured $\mathbf{f}_o(\mathbf{x}_t, \mathbf{u}_t)$, under mild conditions, can be rewritten in the control-affine form (2.1) according to the procedure detailed in [67]. Furthermore, we assume (2.1) is a time-sampled version of its continuous-time counterpart, whose existence is guaranteed for a large class of forward-complete systems, e.g., mechanical systems [55].

Approach. Inspired by operator-theoretic dynamical system theory, we consider modeling of (2.1) as a bilinear dynamical surrogate system evolving in the RKHS \mathcal{H} as³

$$(2.2) \quad \mathbf{z}_{t+1} = A^\top \mathbf{z}_t + \sum_{j=1}^{n_u} B_j^\top u_j(t) \mathbf{z}_t$$

where $\mathbf{z}_t \in \mathcal{H}_X$ so the dynamics are modeled by bounded linear operators $A : \mathcal{H}_X \rightarrow \mathcal{H}_X$ and $\{B_j : \mathcal{H}_X \rightarrow \mathcal{H}_X\}_{j \in [n_u]}$. We pose the construction of a finite-dimensional realization of (2.2) as a *control-Koopman operator regression* problem for $G : \mathcal{H}_U \rightarrow \mathcal{H}_X$. In particular, we assume that \mathcal{H}_X and \mathcal{H}_U are RKHSs with associated canonical feature maps $k_{\mathbf{x}} : \mathbb{X} \rightarrow \mathcal{H}_X$ and $k_{\mathbf{x}, \mathbf{u}} : \mathbb{X} \times \mathbb{U} \rightarrow \mathcal{H}_U$ on the data spaces \mathbb{X} and $\mathbb{X} \times \mathbb{U}$, respectively.

We consider solving the following control-operator regression problem

$$(COP) \quad \min_{G \in \mathcal{B}(\mathcal{H}_U, \mathcal{H}_X)} \|k_{\mathbf{x}_+} - G^\top k_{\mathbf{x}, \mathbf{u}}\|_{L_2(\mathcal{H}_X)}^2$$

where $\mathcal{B}(\mathcal{H}_U, \mathcal{H}_X)$ is the space of bounded operators from \mathcal{H}_U to \mathcal{H}_X . Together with solving a *control operator problem* (COP), we consider the recovery of the state-space model (2.1) via a *reconstruction problem*

$$(RP) \quad \min_{C \in \mathcal{B}(\mathcal{H}_X, \mathbb{X})} \|\mathbf{x} - C^\top k_{\mathbf{x}}\|_{L_2(\mathbb{X})}^2$$

³While such a disparity is disregarded in control systems literature [49], we highlight the adjoint because state-space models formally evolve the basis of a Hilbert space using the dual embedded operators, cf. [47].

where the observable of particular interest is the identity function⁴. In contrast to the RKHS literature focused on the eigendecomposition of a Koopman operator estimate [47], we focus on full rank estimators. If low-rank constraints are desired, the framework we propose is fully compatible with principal component and reduced rank estimators [94, 93, 54] as it presents a natural counterpart to existing Koopman operator regression for control systems.

Objective. *The aim of this work is to learn (2.1) using a dataset of snapshot pairs*

$$(2.3) \quad \mathbb{D}_N = \left\{ \underbrace{\mathbf{x}_{t_i+1}, \mathbf{x}_{t_i}, \mathbf{u}_{t_i}}_{\mathbf{f}(\mathbf{x}_{t_i}, \mathbf{u}_{t_i})} \right\}_{i \in [N]} = \left\{ \mathbf{x}_+^{(i)}, \mathbf{x}^{(i)}, \mathbf{u}^{(i)} \right\}_{i \in [N]}$$

via a bilinear predictor of the form

$$(2.4a) \quad \mathbf{z}_{t+1} := \widehat{\mathbf{A}}^\top \mathbf{z}_t + \sum_{j=1}^{n_u} \widehat{\mathbf{B}}_j^\top u_j(t) \mathbf{z}_t$$

$$(2.4b) \quad \hat{\mathbf{x}}_t = \widehat{\mathbf{C}}^\top \mathbf{z}_t$$

where estimating $(\widehat{\mathbf{A}}, \widehat{\mathbf{B}}, \widehat{\mathbf{C}})$:

1. Follows from a empirical risk minimization (ERM);
2. Avoids the curse of feature and input dimensionality;
3. Is compatible with established ERM operator estimators for (COP);
4. Can be efficiently performed for large datasets \mathbb{D}_N using random projections.

3. Koopman operator theory, representations and control systems.

3.1. Koopmanism. First, let's consider the autonomous case with

$$(3.1) \quad \mathbf{x}_{t+1} = \mathbf{f}(\mathbf{x}_t)$$

where \mathbf{f} is Lipschitz continuous, $\mathbf{x}_t \in \mathbb{X}$, and $\mathbb{X} \subset \mathbb{R}^{n_x}$ is compact. The Koopman operator corresponding to the dynamics (3.1) is $\mathcal{A} : \mathcal{F} \mapsto \mathcal{F}$, which advances the underlying state one time step further by composing the dynamics with the observable $\psi : \mathbb{X} \mapsto \mathbb{C}$ as

$$(3.2) \quad \mathcal{A}\psi(\mathbf{x}_t) = \psi(\mathbf{f}(\mathbf{x}_t)) = \psi(\mathbf{x}_{t+1}),$$

where \mathcal{F} – the functional space of the observables – is considered to be the Hilbert space of continuous square-integrable functions $\psi \in \mathcal{F} := \mathcal{C}(\mathbb{X}) \cap L^2(\mathbb{X})$. Observables (also known as lifting/measurement functions) are state-dependent functions that lift the dynamics (3.1) to an infinite-dimensional space, where the state-transition map is defined by a linear operator. Due to (3.1) being a well-defined sampled version of a continuous-time system, implies that the family $\{\mathcal{A}_t \equiv (\mathcal{A})^t\}_{t \in \mathbb{N}}$ forms a semigroup.

The appeal of Koopman operators lies in their ability to *linearize* the underlying dynamical system (3.1) by linearly representing dynamics in terms of functionals instead of points in \mathbb{X} . While they admit a spectral decomposition due to being bounded for Lipschitz dynamics

⁴One may set any function of interest but focus on the full-state observable to build a surrogate for (2.1).

[56], it is generally not true that a finite-rank representation can adequately capture all of the dynamics of a nonlinear system. This is due to the fact that operator spectra comprises not only of a point spectrum but also a continuous and residual spectrum $\sigma(\mathcal{L}) = P_\sigma(\mathcal{L}) \cup C_\sigma(\mathcal{L}) \cup R_\sigma(\mathcal{L})$ where \mathcal{L} denotes the Koopman operator generator (Lie derivative). Note that the sole presence of a points spectrum is essential for a finite-rank LTI dynamics representation.

The flexibility of a non-recurrent domain. A particularly general setting for deterministic dynamics is one concerning with nonlinear dynamics of transient states on the way to a stable solution, which can be completely described by Koopman operator eigenfunctions [22, Chapter 31]. For deterministic systems on such a transient/non-recurrent domain $\mathbb{X}_{[T]} \subset \mathbb{X}$, we can rule out the presence of continuous and residual spectra $C_\sigma(\mathcal{L}) = R_\sigma(\mathcal{L}) = \emptyset$ [11, 9]. Hence, the Koopman operator has a rich (arbitrary) point spectrum [50] defining left eigenvalue-eigenfunction pairs $(\lambda_i, \phi_i) \subseteq \mathbb{C} \times \mathcal{F}_{[T]}$, such that⁵ $\mathcal{A}_{[T]}\phi_i = \lambda_i\phi_i$, $\mathcal{A}_{[T]}^\top\phi_i^\top = \lambda_i^\top\phi_i^\top$ so that $\langle \phi_i^\top, \phi_i \rangle = 1$. Thus, we can represent the operator in the following form

$$(3.3) \quad \mathcal{A}_{[T]}^t = \sum_{i=1}^{\infty} \lambda_i^t \phi_i \otimes \phi_i^\top.$$

Crucially, a finite collection of *open eigenfunctions* $\Phi = \text{vec}(\{\phi_i\}_{i \in \mathbb{N}})$ [62] can approximate any continuous function \mathbf{f} to arbitrary precision [52, 9]. This way, the nonlinear dynamics (3.1) admits a universal representation $\sup_{\mathbf{x}_0 \in \mathbb{X}_{[T]}} |\mathbf{x}_t - \hat{\mathbf{x}}_t| \leq \epsilon$ for $t \in [0, T]$ via an LTI system

$$(3.4a) \quad \Phi_t = (\mathbf{A}^\top)^t \Phi_0$$

$$(3.4b) \quad \hat{\mathbf{x}}_t = \mathbf{C}^\top \Phi_t$$

that allows for greatly simplified multi-step prediction (forecasting). The above representation is demonstrated to be a useful setting for learning of dynamical systems [9] as the operator can be replaced by a finite-dimensional LTI system (3.4), beyond the known one for compact operators associated with time-symmetric stochastic dynamics [54].

Remark 3.1 (Non-recurrence escapes impossibilities and limitations). Recently in [58], it is shown that nonlinear systems with more than one ω -limit sets, e.g. multiple fixed-points, cannot admit a continuous eigenmap basis. The non-recurrent domain defines a subset of the state-space that excludes singularities [11], elegantly allowing for continuous eigenmaps defining the LTI dynamical system (3.4) for a finite-time horizon $t \in [0, T]$. The non-recurrent domain also ensures that Φ is injective [9] – guaranteeing the existence of a left inverse. The latter, together with the denseness in the space of continuous functions, leaves little justification for nonlinear left inverses [72, 70] in place of (3.4b) unless significant dimensionality reduction is desired.

3.2. Koopman-based control system representations. While necessary and sufficient conditions [13] are established for continuous-time dynamics [32, 33] to admit an exact bilinear representation, their discrete-time counterparts are not as well understood. As shown in [42],

⁵We highlight the dependence of operators on a non-recurrent domain by the subscript $(\cdot)_{[T]}$ to denote the finite-time/transient nature of the non-recurrent domain.

there is an exact finite-dimensional embedding for a particular class of systems. Nevertheless, it is unknown that under what conditions infinite-dimensional “bilinearizability” holds for general *discrete-time control-affine* systems. It is also an open question how to obtain a data-driven realization that can effectively work in spaces that can satisfy *bilinearizability* conditions similar to those of the from [13] that directly work out in discrete-time.

3.2.1. Control-Koopman operators. Tractably working with infinite-dimensions through an RKHS approach has various benefits, e.g., overcoming slow modes of convergence [98] of parametric projection approaches [69, 83, 76] that aim at data-driven approximations of Galerkin methods. Before we demonstrate how universal control-affine RKHSs allow for a practical way of dealing with infinite-dimensional bilinear dynamics, we take a step back and show a generic result regarding bilinearizability. This allows us to push the commonly considered input-dependence of Koopman operators entirely into its domain when the underlying dynamics are control-affine and considered on a non-recurrent domain.

Lemma 3.2 (Control-affine systems admit exact bilinear dynamics). *Consider a control-affine system (2.1) on a compact non-recurrent domain $\mathbf{x}_t \in \mathbb{X}_{[T]} \subset \mathbb{X}$, and compact input domain $\mathbb{U} \subset \mathbb{R}^{n_u}$. Assume $\mathbf{h} = \text{id}$, $\mathbf{f}, \{\mathbf{g}_j\}_{j=1}^{n_u} \in \mathcal{F}_{[T]}$. Then, (2.1) admits an exact representation of the dynamics in $\mathcal{F}_{[T]}$ of the form*

$$(3.5a) \quad \Phi_{t+1} \equiv \mathcal{A}_{[T]}^\top(\mathbf{u})\Phi_t = \mathcal{A}_{[T]}^\top\Phi_t + \sum_{j=1}^{n_u} \mathcal{B}_{[T]_j}^\top\Phi_t u_{j,t}$$

where $\Phi \in \text{span}(\{\phi_i\}_{i=1}^\infty) \equiv \mathcal{F}_{[T]}$, $U_j = \text{diag}(\{u_j^{(i)}\}_{i=1}^\infty)$, $\mathbb{U} \equiv \{[u_1^{(i)} \ \dots \ u_{n_u}^{(i)}]^\top\}_{i=1}^\infty$, $\phi_i^{t+1} = \lambda_i \phi_i^t$ with $\lambda_i \in \mathbb{C}$ and $\mathcal{A}_{[T]} \equiv \text{diag}(\{\lambda_i\}_{i=1}^\infty)$.

Proof. With all components (2.1) spanned by Koopman eigenmaps by assumption and $\mathcal{A}_{[T]}\mathcal{F}_{[T]} \subseteq \mathcal{F}_{[T]}$ by construction, the dynamics obviously stay control-affine in Φ . Thus, there exists an operator of the following form

$$(3.6a) \quad \mathcal{A}_{[T]}(\mathbf{u}) = \sum_{i=1}^\infty \lambda_i \phi_i \otimes \phi_i^\top + \sum_{j=1}^{n_u} u_j \sum_{i=1}^\infty \lambda_i \phi_i \otimes (\phi_i^\top \otimes u_j^{(i)})$$

By boundedness of $\mathcal{A}_{[T]}$ and control inputs

$$(3.6b) \quad = \sum_{i=1}^\infty \lambda_i \phi_i \otimes \phi_i^\top + \sum_{i=1}^\infty \sum_{j=1}^{n_u} u_j \lambda_i \phi_i \otimes (\phi_i^\top \otimes u_j^{(i)})$$

$$(3.6c) \quad = \sum_{i=1}^\infty \lambda_i \phi_i \otimes \left(\phi_i + \sum_{j=1}^{n_u} (\phi_i^\top \otimes u_j^{(i)}) u_j \right)$$

$$(3.6d) \quad \stackrel{\text{plug in (3.3)}}{=} \mathcal{A}_{[T]} + \sum_{j=1}^{n_u} \mathcal{A}_{[T]} U_j u_j$$

$$(3.6e) \quad = \mathcal{A}_{[T]} + \sum_{j=1}^{n_u} \mathcal{B}_{[T]_j} u_j \quad \blacksquare$$

Exactly spanning the autonomous and control dynamics might seem to be a strong assumption. However, even when the assumption is violated, the representation can get arbitrarily accurate for (2.1) with continuous functions as we formalize in the following corollary.

Corollary 3.3 (Universality). *Consider $\mathcal{F}_{[T]} := \text{span}(\{\phi_i\}_{i=1}^\infty)$ with $\phi_i^{t+1} = \lambda_i \phi_i^t$. Then, for every continuous $\mathbf{h} := \text{id}(\cdot)$, $\mathbf{f}, \{\mathbf{g}_j\}_{j=1}^{n_u}$ over a non-recurrent domain $\mathbb{X}_{[T]}$ and all $\epsilon_x, \epsilon_f, \{\epsilon_{g_j}\}_{j=1}^{n_u} > 0$, there exist $\tilde{\mathbf{h}}, \tilde{\mathbf{f}}, \{\tilde{\mathbf{g}}_j\}_{j=1}^{n_u} \in \mathcal{F}_{[T]}$ so that $\|\tilde{\mathbf{h}} - \mathbf{h}\|_\infty \leq \epsilon_x$, $\|\tilde{\mathbf{f}} - \mathbf{f}\|_\infty \leq \epsilon_f$, $\{\|\tilde{\mathbf{g}}_j - \mathbf{g}_j\|_\infty \leq \epsilon_{g_j}\}_{j=1}^{n_u}$.*

Proof. Follows directly by using the fact that $\mathcal{F}_{[\tau]}$ is dense in the set of continuous functions $\mathcal{C}(\mathbb{X}_{[\tau]})$ over a non-recurrent domain $\mathbb{X}_{[\tau]}$ [52]. ■

Remark 3.4 (Choice of observables). While we rigorously show novel existence results, one might question if they can be realized in practice. The answer is positive, as recent literature provides explicit *necessary and sufficient* conditions [9, Lemma 1] to work in a space $\mathcal{F}_{[\tau]} \equiv \text{span}(\{\phi_i\}_{i=1}^{\infty})$ consisting solely of Koopman (open) eigenfunctions [62]. Even when less care is taken, i.e. by not explicitly working in invariant subspaces, *universal RKHS* [43] can make the residual error of not working in an invariant subspace arbitrarily small [54, 53]. We formalize this fact in the subsequent section after formulating the infinite-dimensional operator regression problem.

With the representational preliminaries in place, we aim to construct their counterpart in a universal RKHS [43]. The *flexibility* our approach comes from the fact that given a universal kernel, neither the feature map nor the feature space are uniquely determined [43] – defining a dictionary-free approach. Nonetheless, an RKHS uniquely defines a kernel (and vice versa) [43], so we enforce the structure of (3.5a) on the feature space of an RKHS to derive a kernel that corresponds to it. As we will see later, such a kernel will be crucial for working with infinite-dimensional spaces in practice.

3.2.2. Control-operator-valued reproducing kernel Hilbert spaces. Now, we can take advantage of the fact that control-affine systems are bilinear in $\mathcal{F}_{[\tau]}$ to pass the dependence on the inputs to the domain of the operators (Theorem 3.5). Then, by deriving the input domain of the RKHS-bound control-Koopman operator $G : \mathcal{H}_U \rightarrow \mathcal{H}_X$, we get a natural analogue to the time-homogeneous case – leading to a superior paradigm compared to the existing parametric approaches from the literature – see Table 1 for an overview. In the following, we exploit the “operator kernel tick” to control systems which elegantly avoids taking tensor products [71, 87], collection of multiple datasets or incurring a loss of precision, i.e. by discretizing the space or inputs before the data comes in.

To set up the estimation of linear control-Koopman operator (3.6) without knowledge of Φ , we consider nonparametric regression using a universal kernel (cf. Remark 3.4) on a linear space consisting of function mappings from $\mathbb{X}_{[\tau]}$ to \mathcal{H}_X [65] given by

$$(3.7) \quad \mathcal{G}_X = \{F \equiv A^\top k_{\mathbf{x}} : \mathbb{X}_{[\tau]} \rightarrow \mathcal{H}_X \mid A : \mathcal{H}_X \rightarrow \mathcal{H}_X \text{ is Hilbert-Schmidt}\}.$$

In what follows, \mathcal{G}_X will always denote the \mathcal{H}_X -valued kernel $K : \mathbb{X}_{[\tau]} \times \mathbb{X}_{[\tau]} \rightarrow \mathcal{B}(\mathbb{X}_{[\tau]})$ given by $K(\mathbf{x}, \mathbf{x}') = k(\mathbf{x}, \mathbf{x}') \text{Id}_{\mathcal{H}_X}$ as described in this section. We will write capital letters $F \in \mathcal{G}_X$ for \mathcal{H}_X -valued functions in order to distinguish them from scalar-valued functions $f \in \mathcal{H}_X$. The foundation of our approach is given by the fact that elements of the RKHS \mathcal{G}_X can be interpreted as Hilbert-Schmidt operators on \mathcal{H}_X , whereas the \mathcal{G}_U can be interpreted as Hilbert-Schmidt operators from \mathcal{H}_U to \mathcal{H}_X . For a concise overview of vector/operator-valued reproducing kernel Hilbert spaces, we point the reader to [64] and to [19] for a more extensive treatment.

Theorem 3.5 (Control-Koopman operator domain). *Consider a universal kernel $k(\mathbf{x}, \mathbf{x}')$ and the bilinear surrogate (3.5) of control-affine dynamics (2.1). Then, the control-endowed RKHS domain for the control-Koopman operator $G|_{\mathcal{H}} : \mathcal{H}_U \rightarrow \mathcal{F}_{[\tau]}$ is identified with the RKHS*

of the kernel

$$(3.8) \quad k((\mathbf{x}, \mathbf{u}), (\mathbf{x}', \mathbf{u}')) = k(\mathbf{x}, \mathbf{x}') + \sum_{j=1}^{n_u} u_j k(\mathbf{x}, \mathbf{x}') u'_j.$$

Proof. Analogously to (3.7), simple rearranging leads to

$$(3.9)$$

$$\mathcal{G}_U = \{G^\top k_{\mathbf{x}, \mathbf{u}} : \mathbb{X}_{[r]} \times \mathbb{U} \rightarrow \mathcal{H}_U \mid G : \mathcal{H}_U \rightarrow \mathcal{H}_X \text{ is Hilbert-Schmidt}\}$$

$$(3.10)$$

$$\stackrel{\text{Lem. 3.2}}{=} \underbrace{\{G^\top (k_{\mathbf{x}} + \sum_{j=1}^{n_u} k_{\mathbf{x}} U_j^\top u_j) : \mathbb{X}_{[r]} \times \mathbb{U} \rightarrow \mathcal{H}_X \oplus (\oplus_{j \in [n_u]} U_j \mathcal{H}_X) \mid G : \text{HS}(\mathcal{H}_U, \mathcal{H}_X)\}}_{:=F_{\mathbf{u}}(\mathbf{x}, \mathbf{u})}.$$

that we can reformulate using the *reproducing property*

$$(3.11a)$$

$$\langle F_{\mathbf{u}}, F'_{\mathbf{u}} \rangle_{\mathcal{G}_U} \stackrel{(3.6d)}{=} \left\langle k_{\mathbf{x}'} + \sum_{j=1}^{n_u} u'_j U_j k_{\mathbf{x}'}, k_{\mathbf{x}} + \sum_{j=1}^{n_u} k_{\mathbf{x}} U_j^\top u_j \right\rangle_{\mathcal{H}_X \oplus (\oplus_{j \in [n_u]} U_j \mathcal{H}_X)} \langle h, h' \rangle_{\mathcal{H}_X}$$

$$(3.11b)$$

$$\stackrel{\text{direct sum}^6 \text{ of RKHSs [2, Sec. 6.]}}{=} \underbrace{\left(k(\mathbf{x}, \mathbf{x}') + \sum_{j=1}^{n_u} u'_j k(\mathbf{x}, \mathbf{x}') u_j \right)}_{=k((\mathbf{x}, \mathbf{u}), (\mathbf{x}', \mathbf{u}'))} \langle h, h' \rangle_{\mathcal{H}_X}$$

$$(3.11c)$$

$$= \langle k((\mathbf{x}, \mathbf{u}), (\mathbf{x}', \mathbf{u}')) \text{Id}_{\mathcal{H}} h, h' \rangle_{\mathcal{H}_X}.$$

Finally, by applying [64, Theorem 4.4] it follows that the operator-valued RKHS given above is induced by (3.8). \blacksquare

By utilizing the operator reproducing property (3.11) and identifying the canonical kernel feature map on \mathcal{H}_X , the operator-valued RKHS least squares regression problem

$$(3.12) \quad \min_{F_{\mathbf{u}} \in \mathcal{G}_U} \mathbb{E} \left[\|k_{\mathbf{x}_+} - F_{\mathbf{u}}(\mathbf{x}, \mathbf{u})\|_{\mathcal{H}_X}^2 \right]$$

is equivalent to

$$(3.13) \quad \min_{G \in \text{HS}(\mathcal{H}_U, \mathcal{H}_X)} \underbrace{\mathbb{E} \left[\|k_{\mathbf{x}_+} - G^\top k_{\mathbf{x}, \mathbf{u}}\|_{\mathcal{H}_X}^2 \right]}_{\mathcal{R}(G)}$$

which obviously coincides with (COP) only now with an input kernel function (3.8) tailored to control-affine systems.

⁶We use \oplus to generally denote the *direct sum* of Hilbert spaces.

Remark 3.6 (Flexibility of our approach). Operator models using structured kernels, like (3.8), must not be confused with parametric models that work with a fixed amount of observables, with a predetermined structure and use a fixed number of parameters. In contrast, our operator regression with a universal, infinite-dimensional, yet structured kernel has potentially infinitely many observables for each part of its bilinear model. So the kernel encodes the knowledge that the target operator is bilinear, but each summand has unlimited flexibility due to a possibly infinite amount of observables.

4. Control-Koopman Operator Regression (cKOR). With the domain \mathcal{H}_U uniquely defined by its kernel, we focus on formulating a well-posed regression problem to solve (COP).

4.1. General concept. To ensure the uniqueness and feasibility of the solution, Tikhonov regularization [17] of problem (3.13) reads as

$$(4.1) \quad G_\gamma = \arg \min_{G \in \text{HS}(\mathcal{H}_U, \mathcal{H}_X)} \underbrace{\|S_+ - S_U G\|_{\text{HS}}^2}_{\mathcal{R}(G)} + \gamma \|G\|_{\text{HS}}^2, \quad \gamma > 0.$$

whose closed-form solution [54] reads as

$$(4.2a) \quad G_\gamma = (C + \gamma I_{\mathcal{H}_X})^{-1} T \quad (\text{input covariance } C, \text{ target cross-covariance } T)$$

$$(4.2b) \quad = (S_U^\top S_U + \gamma I_{\mathcal{H}_X})^{-1} S_U^\top S_+$$

$$(4.2c) \quad \stackrel{7}{=} S_U^\top (K_U + \gamma I_{\mathcal{H}_X})^{-1} S_+$$

$$(4.2d) \quad \stackrel{\text{Thm. 3.5}}{=} (S^\top + \sum_{j=1}^{n_u} S^\top U_j^\top) \left(K + \sum_{j=1}^{n_u} U_j K U_j^\top + \gamma I_{\mathcal{H}_X} \right)^{-1} S_+$$

$$(4.2e) \quad = A_\gamma + \sum_{j \in n_u} B_{\gamma_j}$$

where S_U and S injection operators, mapping from RKHS to $\mathcal{F}_U = \mathcal{S}(\mathcal{F} \oplus (\bigoplus_{j \in [n_u]} U_j \mathcal{F}))$ and \mathcal{F} , respectively, where

$$(4.3) \quad \mathcal{S}: \mathcal{F}_U \rightarrow \mathcal{F} \mid (f \ u_1 g_1 \ \cdots \ u_{n_u} g_{n_u}) \mapsto f + u_1 g_1 + \dots + u_{n_u} g_{n_u}$$

is a summation operator.

Rationale on the regression task. Given a universal kernel $\mathcal{H}_X \subseteq L^2(\mathbb{X}_{[T]})$, the injection S is Hilbert-Schmidt (HS) [43]. Thus, the restriction of the Koopman operator $S_+ := \mathcal{A}_{[T]}(\mathbf{u})S$ is also HS, by virtue of the control Koopman operator $\mathcal{A}_{[T]}(\mathbf{u})$ being bounded – providing a well-defined regression task.

For the bilinear input effects, the kernel (injection operator) structure (3.8) is critical, so a single inversion of the stabilized Gram operator K_U delivers

$$(4.4) \quad A_\gamma = S^\top (K_U + \gamma I_{\mathcal{H}_X})^{-1} S_+$$

$$(4.5) \quad \{B_{\gamma_j} = U_j^\top S^\top (K_U + \gamma I_{\mathcal{H}_X})^{-1} S_+\}_{j \in [n_u]}$$

defining control-affine parts of the infinite-dimensional bilinear dynamics (2.2).

⁷Matrix identity $(S_U^\top S_U + \gamma I_{\mathcal{H}_X})^{-1} S_U^\top = S_U^\top (S_U S_U^\top + \gamma I_{\mathcal{H}_X})^{-1} +$ “kernel trick” $S_U S_U^\top = K_U$

Remark 4.1 (Discretized only by data). It is important to stress that the above solution is equivalent to a vector-valued representer theorem [18] due to the equivalence of vector-valued regression [1] and sampling operator formalism [54, 53, 59]. While intractable, the above representations allows for direct expressions for the infinite-dimensional A_γ and B_γ operators, without a loss of precision via discretizing the space and inputs as in existing literature [76, 69, 77, 77, 83].

Next, we assess the approximation capability and well-posedness of the regression problem when data samples are introduced and we derive tractable data-driven estimators.

4.2. Approximations of control-Koopman operators in RKHS. Now that we have set up control-Koopman operator representations both in the space of continuous elements of L^2 as well as in RKHS, we investigate the approximation capabilities of an RKHS representation w.r.t. the one in $\mathcal{F}_{[\tau]}$. This is of great importance in assessing whether or not we can recover the true control-Koopman operator or get close to it in a well-posed manner.

Well-specified case. When \mathcal{H}_X is an invariant subspace of $\mathcal{A}_{[\tau]}$ up to its closure $\text{Im}(S_+) = \text{cl}(\text{Im}(S_U)) \subseteq L^2(\mathbb{X}_{[\tau]})$, then, there exists a $G \in \text{HS}(\mathcal{H}_U, \mathcal{H}_X)$ fulfilling the target operator equation $k_{\mathbf{x}_+} = G^\top k_{\mathbf{x}, \mathbf{u}} \Leftrightarrow S_+ = S_U G$ so the error vanishes $G = (S_U^\top S_U)^\dagger S_U^\top S_+ = \lim_{\gamma \rightarrow 0} G_\gamma \implies A = \lim_{\gamma \rightarrow 0} A_\gamma, B = \lim_{\gamma \rightarrow 0} B_\gamma$, where $(\cdot)^\dagger$ denotes the Moore-Penrose pseudoinverse operator [86]. Working with invariant subspaces – ensuring $\mathcal{G}_{[\tau]} \in \text{HS}(\mathcal{H}_U, \mathcal{H}_X)$ – can be realized through a kernel function reflecting known invariant-subspaces of classes of polynomial systems [41] or using invariance-transformations [9].

Misspecified case. When the RKHS does not admit a Hilbert-Schmidt control-Koopman operator – $A_0 \notin \text{HS}(\mathcal{H}_X, \mathcal{H}_X) \Leftrightarrow G_0 \notin \text{HS}(\mathcal{H}_U, \mathcal{H}_X)$ – one cannot define G_0 from \mathcal{H}_U to \mathcal{H}_X . However, G_γ is consistent with the control-Koopman operator $\mathcal{G}_{[\tau]}$ from \mathcal{H}_U to \mathcal{H}_X and by extension so are A_γ and $\{B_{\gamma_k}\}_{k \in n_{\mathbf{u}}}$ with $\mathcal{A}_{[\tau]}$ and $\{\mathcal{B}_{[\tau]_k}\}_{k \in n_{\mathbf{u}}}$, respectively, if γ is set small enough [54].

4.3. Estimating control-Koopman operator from data. While in the previous section, we derived the infinite-dimensional solution of the problem at hand, now we derive a practical finite-dimensional representation using a dataset (2.3) so that (3.13) is approximately solved via regularized empirical risk minimization (RERM). In this work, we consider the following convex optimization problem

$$\text{(RERM)} \quad \hat{\mathbf{G}}_\gamma := \arg \min_{\mathbf{G} \in \text{HS}(\mathcal{H}_U, \mathcal{H}_X)} \underbrace{\frac{1}{N} \sum_{i=1}^n \|\hat{S}_+ - \hat{S}_U \mathbf{G}\|_{\text{HS}}^2}_{\hat{\mathcal{R}}^\gamma(\mathbf{G})} + \gamma \|\mathbf{G}\|_{\text{HS}}^2,$$

where $\gamma > 0$ is the regularization parameter and $\hat{S}_{(\cdot)}$ the empirical injections called sampling operators – see Appendix A for a detailed derivation including operator estimators based on *kernel ridge regression* (KRR), *principal component regression* (PCR) – a popular DMD technique – and recently proposed *reduced rank regression* (RRR). Next, we only state the result for kernel ridge-regression (KRR) as this estimator will be further used in this work. For that, we introduce the shorthands $\mathbf{K} := \hat{S} \hat{S}^\top = [k(\mathbf{x}^{(i)}, \mathbf{x}^{(j)})]_{i,j \in [N]}$, $\mathbf{U}_k := \text{diag}([u_k^{(1)} \cdots u_k^{(N)}])$ and $\mathbf{K}_+ := \hat{S}_+ \hat{S}_+^\top = [k(\mathbf{x}_+^{(i)}, \mathbf{x}_+^{(j)})]_{i,j \in [N]}$.

Theorem 4.2 (Control-Koopman Operator KRR). *The minimizer of (RERM) is the compound sum of operators*

$$\widehat{\mathbf{G}}_\gamma = \widehat{\mathbf{A}}_\gamma + \sum_{k \in [n_u]} \widehat{\mathbf{B}}_{\gamma_k}$$

where the estimated state $\widehat{\mathbf{A}}_\gamma$ and input transfer operators $\widehat{\mathbf{B}}_{\gamma_k}$ are defined as

$$(4.6a) \quad \widehat{\mathbf{A}}_\gamma = (\mathbf{K} + \sum_{k \in [n_u]} \mathbf{U}_k \mathbf{K} \mathbf{U}_k^\top + \gamma \mathbf{I})^{-1} \mathbf{K}_+$$

$$(4.6b) \quad \{\widehat{\mathbf{B}}_{\gamma_k} = \mathbf{U}_k^\top \widehat{\mathbf{A}}_\gamma\}_{k \in [n_u]}$$

defining the bilinear model for our objective (2.4a).

Proof. Using Theorem 3.5, and the symmetry of the input sampling operators, the full KKR estimator directly follows after exchanging outer sampling operators by a fully-kernelized matrix description \mathbf{K}_+ using [47, Proposition 3.1]. \blacksquare

Although we focus on the well-justified bilinear representations, our cKOR framework includes many existing representations in a nonparametric manner as summarized in Table 2. We are unaware of existing methods other than our work considering operator-theoretic learning of control systems to a comparable level of generality.

Table 2: Popular representations of existing Koopman-operator representations for control systems. Consider that $k_{\mathbf{x}}$ are canonical features of a possibly infinite-dimensional RKHS. *cKOR* includes all control-affine representations with straightforward modification of sampling operators in Appendix A.

Method	Embedding dynamics	Input kernel $\langle \cdot, \cdot \rangle_{\mathcal{H}_U}$	Output kernel $\langle \cdot, \cdot \rangle_{\mathcal{H}_X}$
DMD [84]	$\mathbf{A}^\top \mathbf{x}$	$\mathbf{x}^\top \mathbf{x}'$	$\mathbf{x}^\top \mathbf{x}'$
DMDc [78]	$\mathbf{A}^\top \mathbf{x} + \mathbf{B}^\top \mathbf{u}$	$\mathbf{x}^\top \mathbf{x}' + \mathbf{u}^\top \mathbf{u}'$	$\mathbf{x}^\top \mathbf{x}'$
k EDMD [47, 94]	$A^\top k_{\mathbf{x}}$	$k(\mathbf{x}, \mathbf{x}')$	$k(\mathbf{x}, \mathbf{x}')$
k EDMDc	$A^\top k_{\mathbf{x}} + B^\top \mathbf{u}$	$k(\mathbf{x}, \mathbf{x}') + \mathbf{u}^\top \mathbf{u}'$	$k(\mathbf{x}, \mathbf{x}')$
cKOR	$A^\top k_{\mathbf{x}} + \sum_{k=1}^{n_u} B_k^\top u_k k_{\mathbf{x}}$	$k(\mathbf{x}, \mathbf{x}') + \sum_{k=1}^{n_u} u_k k(\mathbf{x}, \mathbf{x}') u_k'$	$k(\mathbf{x}, \mathbf{x}')$

5. Efficient approximations via sketching. Like any other nonparametric approach, our cKOR algorithm is only suitable for small-scale systems due to the time-complexity of order $\mathcal{O}(N^3)$ w.r.t. the data cardinality N . For approximating nonparametric methods, random Fourier features (RFFs) stand out as a popular and straightforward way to reduce the estimators' complexity [81]. Recently, they have been utilized for control system identification [77]. Unfortunately, the algorithm in [77] is hardly useful in practice due to requiring data gathered under constant inputs to estimate the Koopman operator for a few fixed input levels – prohibiting most realistic system identification scenarios that involve rich excitation signals or safe data collection, e.g., under an auxiliary controller. Due to RFFs being data-independent, they may not adapt well to the data at hand [95], limiting performance for an equivalent complexity as sketching schemes [20] as the Nyström method selects a subset of training examples to form its basis functions, resulting in a data-based representation.

Random sketching or Nyström approximations estimate the kernel matrix by selecting a small subset of m data points known as inducing points or Nyström centres, that define a low-dimensional subspace of the RKHS the dataset is projected to [92, 1]. The Nyström approximation is accurate under the assumptions that an appropriate sampling is carried out and the kernel matrix has a low rank, where the latter is often satisfied, e.g., for Gaussian kernels whose Gram matrix eigenvalue spectrum rapidly decays [91].

We remark that, concurrent to our work, [16] studies sketched operator estimation, but only for the restrictive case of LTI lifted dynamics that is recovered as a special case of our approach (cf. Table 2).

Complexity independent of input dimensionality. To put our developments in perspective, recall that the popular parametric bEDMD [12] or [34] have the time-complexity of $\mathcal{O}(n_z^3(n_u + 1)^3)$ due to a cubic magnification of complexity in case of control systems based on the dimensionality of the inputs. This is primarily due to a lack of *kernel trick* for the control-affine effects – an inherent limitation of a parametric model. In contrast, the proposed combination of our nonparametric cKOR framework and random sketching that we will work out in this section preserves the control-affine kernel trick at the inducing points and delivers a handy complexity reduction that is *independent of input-dimensionality*, in turn, amounting to the time-complexity of $\mathcal{O}(m^3 + m^2N)$ – identical to the one known for autonomous systems [59].

We will consider uniform random sampling because it is a simple algorithm that is generally applicable and it is well-known that random projections are suitable for extracting a low rank matrix approximation [88]. There exist more advanced sampling approaches, which have the potential to minimize the number of inducing points necessary, but reviewing these methods are out of scope for this work. Importantly, the proposed scalable estimators are not limited to uniform random sampling.

Among sampling-based methods, the concept of Nyström approximation is rigorously studied in context of KOR with KRR, PCR and RRR, in [59]. In the remainder of this section, this method is extended for control-Koopman operator regression. This approach starts by sampling a small subset of the data matrices, i.e. $\tilde{\mathbb{X}} \subset \mathbb{X}$, $\tilde{\mathbb{X}}_+ \subset \mathbb{X}_+$ and $\tilde{\mathbb{U}} \subset \mathbb{U}$ with m datapoints/columns, where $m \ll N$ is the number of inducing points. With these datasets, the *subsampling operators* $\tilde{S}, \tilde{S}_+ : \mathcal{H}_X \rightarrow \mathbb{R}^m$ and $\tilde{S}_U : \mathcal{H}_U \rightarrow \mathbb{R}^m$ are introduced to explicitly represent the orthogonal projection operators onto the reduced span of these operators (compared to their full counterparts). The orthogonal projectors P_+ and P are defined as

$$(5.1) \quad P_+ = \tilde{S}_+^\top (\tilde{S}_+^\top)^\dagger, \quad P = \tilde{S}_U^\top (\tilde{S}_U^\top)^\dagger.$$

where \dagger denotes the Moore-Penrose pseudoinverse. With these projection operators, the original problem (**ERM**) is projected onto a lower-dimensional counterpart by projecting the input and target cross-covariance \hat{C}, \hat{T} as

$$(5.2) \quad \hat{G}_{m,\gamma} = (P\hat{C}P + \gamma I)^{-1} P\hat{T}P_+.$$

As we work with infinite-dimensional $\mathcal{H}_X, \mathcal{H}_U$, the above expression is obviously intractable. Thus, in the following, we derive a commutable version of the estimator using the “kernel trick” with the help of kernel matrix shorthands:

$$\mathbf{K}_{\mathbf{u}\tilde{\mathbf{u}}} := [k((\mathbf{x}, \mathbf{u})^{(i)}, (\tilde{\mathbf{x}}, \tilde{\mathbf{u}})^{(j)})]_{\substack{i \in [N], \\ j \in [m]}}, \mathbf{K}_{\tilde{\mathbf{u}}\tilde{\mathbf{u}}} := [k((\tilde{\mathbf{x}}, \tilde{\mathbf{u}})^{(i)}, (\tilde{\mathbf{x}}, \tilde{\mathbf{u}})^{(j)})]_{\substack{i, j \in [m]}}, \mathbf{K}_{\tilde{\mathbf{x}}_+ \tilde{\mathbf{x}}_+} := [k(\tilde{\mathbf{x}}_+^{(i)}, \tilde{\mathbf{x}}_+^{(j)})]_{\substack{i, j \in [m]}}, \\ \mathbf{K}_{\mathbf{x}_+ \tilde{\mathbf{x}}_+} := [k(\mathbf{x}_+^{(i)}, \tilde{\mathbf{x}}_+^{(j)})]_{\substack{i \in [N], \\ j \in [m]}}, \mathbf{K}_{\tilde{\mathbf{x}}_+ \tilde{\mathbf{x}}_+} := [k(\tilde{\mathbf{x}}_+^{(i)}, \tilde{\mathbf{x}}_+^{(j)})]_{\substack{i, j \in [m]}}, (\mathbf{U}_m)_k := \text{diag}([u_k^{(1)} \cdots u_k^{(m)}]).$$

Proposition 5.1 (Nyström/Sketched cKOR-KRR). *The sketched estimators remain a compound sum of operators*

$$\hat{\mathbf{G}}_{m, \gamma} = \hat{\mathbf{A}}_{m, \gamma} + \sum_{k \in [n_{\mathbf{u}}]} (\hat{\mathbf{B}}_{m, \gamma})_k$$

where the estimated state $\hat{\mathbf{A}}_{m, \gamma}$ and input operators $(\hat{\mathbf{B}}_{m, \gamma})_k$ are defined as

$$(5.3a) \quad \hat{\mathbf{A}}_{m, \gamma} = (\mathbf{K}_{\mathbf{u}\tilde{\mathbf{u}}}^\top \mathbf{K}_{\mathbf{u}\tilde{\mathbf{u}}} + \gamma \mathbf{K}_{\tilde{\mathbf{u}}\tilde{\mathbf{u}}})^{-1} \mathbf{K}_{\mathbf{u}\tilde{\mathbf{u}}}^\top \mathbf{K}_{\mathbf{x}_+ \tilde{\mathbf{x}}_+} \mathbf{K}_{\tilde{\mathbf{x}}_+ \tilde{\mathbf{x}}_+}^{-1} \mathbf{K}_{\tilde{\mathbf{x}}_+ \tilde{\mathbf{x}}_+},$$

$$(5.3b) \quad \{(\hat{\mathbf{B}}_{m, \gamma})_k\}_{k \in [n_{\mathbf{u}}]} = (\mathbf{U}_m^\top)_k \hat{\mathbf{A}}_{m, \gamma}$$

defining the bilinear model for our objective (2.4a).

Proof. Following the proof for Theorem 4.2, the result follows analogously as in [59, Proposition 3.1]. ■

The inverses in Ny-cKOR only take $\mathcal{O}(m^3)$ time, which is a significant improvement compared to $\mathcal{O}(N^3)$, since $m \ll N$. This also holds for solving the reconstruction problem (RP), e.g., it is easy to see that it resembles the multivariate kernel regularized least squares with Nyström projection [82].

6. Model order reduction. For cKOR and Ny-cKOR, the lifted state dimension scales with the dataset cardinality N and inducing points m , respectively. Even for a relatively small number of inducing points compared to the number of datapoints, the lifted state dimension can be too high, e.g., in context of efficient control design or real-time execution on low-level hardware. Therefore, this section explores model reduction opportunities to reduce the lifted state dimension of cKOR and Ny-cKOR.

A compelling approach for ordering and reducing the lifted states is based on proper orthogonal mode decomposition (POD), because it has been successfully applied in obtaining low-dimensional representations based on large-scale datasets in many applications [21]. The dynamic mode decomposition (DMD) algorithm actually makes use of this reduction [85] and surprisingly, this has not been applied to Koopman modelling for control-affine systems – with the exception of DMDc [79] – to the best of the authors' knowledge. POD in DMD, involves taking an SVD of the state data matrix, which ranks the orthogonal structures of this matrix based on the singular values. With this ranking, the r dominant modes/coordinates can be selected to describe the dynamical behaviour of the underlying system. The same reasoning can be applied to cKOR in the lifted space, with the assumption that the dominant coordinates for representing the lifted system correspond to representing the original system.

The aforementioned reduction approach in the context of cKOR (and Ny-cKOR), starts by taking the r -truncated SVD of the kernel matrix

$$(6.1) \quad \llbracket \mathbf{K} \rrbracket_r = \mathbf{V}_r \boldsymbol{\Sigma}_r \mathbf{V}_r^\top,$$

with the POD modes $\mathbf{V}_r \in \mathbb{R}^{N_z \times r}$ and the singular values matrix $\boldsymbol{\Sigma}_r = \text{diag}(\sigma_1, \dots, \sigma_r)$. With these POD modes, the original bilinear lifted system can be transformed into the following

reduced bilinear lifted form

$$(6.2a) \quad \mathbf{z}_r(t+1) = \mathbf{A}_r^\top \mathbf{z}_r(t) + \sum_{j=1}^{n_u} (\mathbf{B}_r^\top)_j u_j(t) \mathbf{z}_r(t),$$

$$(6.2b) \quad \mathbf{x}_t = \mathbf{C}_r^\top \mathbf{z}_r(t),$$

where $\mathbf{z}_r \in \mathbb{R}^r$ represents the reduced lifted states. The reduced lifted states and the corresponding lifted state-transition matrix $\mathbf{A}_r^\top \in \mathbb{R}^{r \times r}$, the control matrices $\{(\mathbf{B}_r^\top)_j \in \mathbb{R}^{r \times r}\}_{j=1}^{n_u}$ and the reconstruction matrix $\mathbf{C}_r^\top \in \mathbb{R}^{n_x \times r}$ are defined as

$$(6.3) \quad \mathbf{z}_r = \mathbf{V}_r^\top \mathbf{z}, \quad \mathbf{A}_r^\top = \mathbf{V}_r^\top \mathbf{A}^\top \mathbf{V}_r, \quad (\mathbf{B}_r^\top)_j = \mathbf{V}_r^\top \mathbf{B}_j^\top \mathbf{V}_r, \quad \mathbf{C}_r^\top = \mathbf{C}^\top \mathbf{V}_r,$$

respectively. Essentially, the aforementioned reduction approach is a truncated POD basis transformation. In context of cKOR, this method is coined as reduced cKOR (r-cKOR). For Ny-cKOR, the reduction approach is identical to cKOR with the difference that the truncated SVD is applied to the kernel matrix $[\mathbf{K}_{\hat{\mathbf{x}}\hat{\mathbf{x}}}]_r$. In this case, the method is coined as reduced Ny-cKOR (r -Ny-cKOR).

In the literature, there is a wealth of possibilities for choosing r for the truncated SVD [29]. An extensive comparison and analysis of such methods is out of the scope of this paper. Here, r is either manually selected or by a percentage threshold τ

$$(6.4) \quad \frac{\sum_{i=1}^r \sigma_i^2}{\sum_{j=1}^N \sigma_j^2} \cdot 100\% \leq \tau,$$

where the singular values are denoted by σ_i .

7. Forecasting and control with cKOR.

7.1. State reconstruction and forecasting. Until now, we focused on the nontrivial control-Koopman operator regression without addressing reconstruction (**RP**). For the full and sketched case, we can introduce finite-dimensional sampling matrices \mathbf{X}, \mathbf{Z} (analogous to sampling operators) as

$$(7.1) \quad \mathbf{X}^\top = [\mathbf{x}^{(1)} \mid \dots \mid \mathbf{x}^{(N)}] \in \mathbb{R}^{n_x \times N} \quad \mathbf{Z}^\top = [\mathbf{z}(\mathbf{x}^{(1)}) \mid \dots \mid \mathbf{z}(\mathbf{x}^{(N)})] \in \mathbb{R}^{N_z \times N},$$

where the mapping $\mathbf{z}(\mathbf{x}^{(i)})$ depends on the data or subsamples for sketching. Then, we can essentially solve an ordinary least squares problem (OLS) minimizing $\|\mathbf{X} - \mathbf{Z}\mathbf{C}\|_{\text{HS}}^2$ with the solution

$$(7.2) \quad \hat{\mathbf{C}} = \mathbf{Z}^\dagger \mathbf{X}$$

While including the state explicitly in a dictionary \mathbf{z} is very popular in the applied literature, we argue against such practice both theoretically and practically in Appendix B, as it can reduce long-term prediction performance by orders of magnitude due the distorting effects it introduces for Koopman operator regression.

Forecasting. With the estimated reconstruction mapping (7.2), we have a fully defined state-space model (2.4) and we can utilize the advantageous bilinear state-space model (2.4) form to have a naturally linear parameter (input) varying (LPV) forecast of our system, with the parameters being the sequence of inputs $\{\mathbf{u}_t\}_{i=0}^{T-1}$. We emphasise that our forecasting model follows an (bi)linear/LPV form at all times, in contrast to works [69, 77] that tacitly employ nonlinear predictors.

7.2. Operator-based LPV-MPC. To provide an efficient scheme for controlling the original nonlinear system via the cKOR method provided surrogate models, we propose a model predictive control (MPC) approach that extends the LPV scheme of [38]. The control problem that we want to address is that given a measurement of the state $\mathbf{x}(t)$ of the original nonlinear system (2.1) at time-instant t , based on a cKOR model of (2.1), solve a predictive control problem for (2.1) on a finite time horizon T with computation cost close to an LTI-MPC to obtain a control sequence $\{\mathbf{u}_{i|t}\}_{i=0}^{T-1}$ such that the predicted response of (2.1) follows a prescribed reference trajectory. Then, $\mathbf{u}_{0|t}$ is applied to the system and at the next time-instant ($t+1$), $\mathbf{x}(t+1)$ is measured to start the next control cycle.

Using the cKOR model, the corresponding optimization problem is shown below

$$\begin{aligned}
(7.3a) \quad & \min_{\mathbf{u}_{0|t} \dots \mathbf{u}_{T-1|t}} \|\mathbf{x}_{T|t} - \bar{\mathbf{x}}_{T|t}\|_{\mathbf{Q}_T}^2 + \sum_{i=0}^{T-1} (\|\mathbf{x}_{i|t} - \bar{\mathbf{x}}_{i|t}\|_{\mathbf{Q}}^2 + \|\mathbf{u}_{i|t} - \bar{\mathbf{u}}_{i|t}\|_{\mathbf{R}}^2) \\
(7.3b) \quad & \text{s.t. } \mathbf{z}_{i+1|t} = \mathbf{A}^\top \mathbf{z}_{i|t} + \mathbf{B}(\mathbf{p}_{i|t}) \mathbf{u}_{i|t} \\
(7.3c) \quad & \mathbf{x}_{j|t} = \mathbf{C}^\top \mathbf{z}_{j|t} \\
(7.3d) \quad & \mathbf{x}_{\min} \leq \mathbf{x}_{j|t} \leq \mathbf{x}_{\max} \\
(7.3e) \quad & \mathbf{u}_{\min} \leq \mathbf{u}_{i|t} \leq \mathbf{u}_{\max}
\end{aligned}$$

where the measured state at time t , i.e., $\mathbf{x}_{0|t} = \mathbf{x}(t)$, is lifted to determine $\mathbf{z}_{0|t} = \mathbf{z}(\mathbf{x}_{0|t})$. The variables $\bar{\mathbf{x}}_{i|t}$ and $\bar{\mathbf{u}}_{i|t}$ correspond to the reference state and input, respectively. In addition, $\mathbf{Q} \in \mathbb{R}^{n_x \times n_x}$, $\mathbf{R} \in \mathbb{R}^{n_u \times n_u}$ are weighting matrices and $\mathbf{Q}_T \in \mathbb{R}^{n_x \times n_x}$ represents the terminal weight matrix. These matrices have to be tuned with respect to user specified performance expectations w.r.t. the tracking problem. The bounds \mathbf{x}_{\min} , \mathbf{x}_{\max} , \mathbf{u}_{\min} and \mathbf{u}_{\max} limit the state and input sequences of the system. Lastly, to efficiently handle the bi-linearity of the cKOR model, a scheduling variable taken as $\mathbf{p}_{i|t}$ is introduced so that

$$(7.4) \quad \mathbf{B}(\mathbf{p}_{i|t}) = [\mathbf{B}_1^\top \mathbf{p}_{i|t} \mid \dots \mid \mathbf{B}_{n_u}^\top \mathbf{p}_{i|t}].$$

The core idea is that, at any given time-instant t , for a fixed scheduling sequence $\{\mathbf{p}_{i|t}\}_{i=0}^{T-1}$, (7.3b) is used to formulate a linear MPC problem that can be solved efficiently as a quadratic program (QP). Then, the resulting control sequence $\{\mathbf{u}_{i|t}\}_{i=0}^{T-1}$ is used to forward simulate the cKOR model to compute a new sequence $\mathbf{p}_{i|t} = \mathbf{z}(i+t)$ on which a new linear MPC problem is formulated and solved. Execution of this iteration multiple times until a converging $\{\mathbf{u}_{i|t}\}_{i=0}^{T-1}$ trajectory is reached ensures that the predictive LPV model (7.3b) sufficiently well approximates the nonlinear system along a (locally) optimal solution trajectory for which the solution of the linear MPC problem coincides with the solution of a nonlinear MPC problem formulated for the original nonlinear model (2.1).

In practice, we solve a single QP at every time-instant where the LPV-MPC updates the scheduling iteratively over the simulation time in a receding horizon manner, which can cause some loss of performance, but still convergence can often be observed in practice, similar to SQP schemes. Details on the implementation are found in Appendix C.

Downsides of linearization-based LPV-MPC. In the LPV literature, these MPC approaches are applied to linearized or factorized models around \mathbf{x}_p and often \mathbf{u}_p as well. In that case, the state-transition matrix is not invariant anymore and the scheduling is not only state-dependent, but often also input-dependent. This input dependence requires a suitably chosen initial input guess in the LPV-MPC algorithm. The reduction of the degrees of freedom combined with a superior approximation advantage of the bilinear Koopman model, make the LPV-MPC based on a bilinear Koopman model a more attractive approach.

Notably, our Koopman LPV-MPC does not require linearization of any form, so the control scheme does not introduce additional approximations into the predictive model used for control design.

8. Numerical experiments. Multiple numerical experiments are presented to illustrate the implications of theoretical results and also demonstrate the advantages of the cKOR approach in combination with a simple yet effective model predictive control scheme based on solving a single QP per timestep.

8.1. Duffing oscillator modelling. As the first example, a controlled damped Duffing oscillator in the state-space form

$$(8.1) \quad \dot{\mathbf{x}} = \begin{bmatrix} x_2 \\ x_1 - x_1^3 - 0.5x_2 \end{bmatrix} + \begin{bmatrix} 0 \\ 2 + \sin(x_1) \end{bmatrix} u.$$

where the state is measured with sampling time $\Delta_t = 0.01s$ and the input is actuated in a synchronised zero-order-hold (ZOH) manner.

Prediction performance for a range of hyperparameters. First we compare the cKOR, Ny-cKOR and the bEDMDC approaches over a range of the hyperparameters $\mu \in \mathbb{R}_+$ of the Gaussian (RBF) kernel

$$(8.2) \quad k(\mathbf{x}, \mathbf{x}') = e^{-1/\mu \|\mathbf{x} - \mathbf{x}'\|_2^2},$$

in terms of the T_{test} -ahead prediction performance, quantified using the root mean square error (RMSE)

$$(8.3) \quad \text{RMSE} = \sqrt{\frac{1}{T_{\text{test}}} \sum_{t=1}^{T_{\text{test}}} \|\mathbf{y}_t - \hat{\mathbf{y}}_t\|_2^2},$$

where N denotes the number of steps and $\mathbf{y}_t - \hat{\mathbf{y}}_t$ the difference between the real and predicted solution. For the training dataset, 200 trajectories with $N = 1000$ samples (10 sec) are generated, starting from a 14 by 14 grid of initial conditions within the limits $|x_1| \leq 2.25$ and $|x_2| \leq 2.25$. For the test dataset, 40 trajectories of $T_{\text{test}} = 100$ samples (1s) are generated, starting from random initial conditions sampled within the limits $|x_1| \leq 2$ and $|x_2| \leq 2$ using a uniform distribution. Both datasets are generated using uniform random input sequences within the interval $[-2, 2]$. From the training dataset, $m = 200$ inducing points are sampled. The considered approaches are used with a regularization parameter $\gamma = N \times 10^{-9}$.

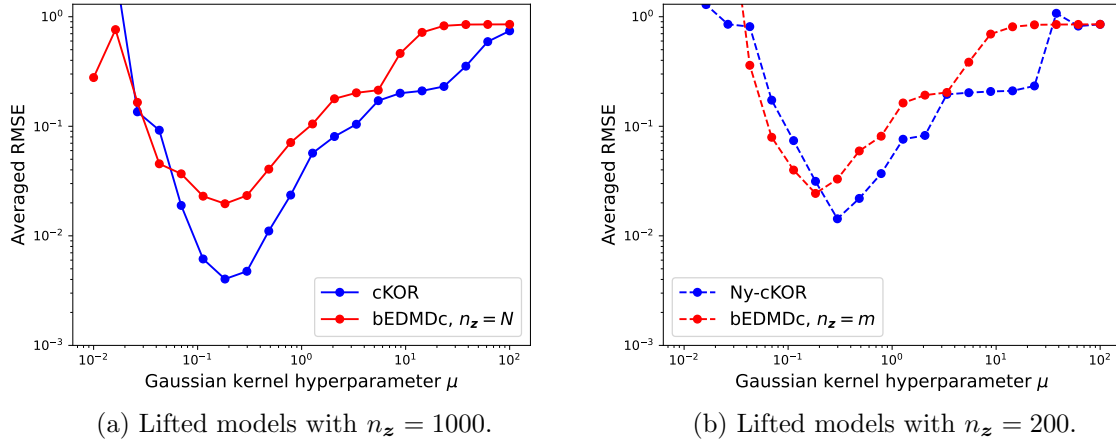
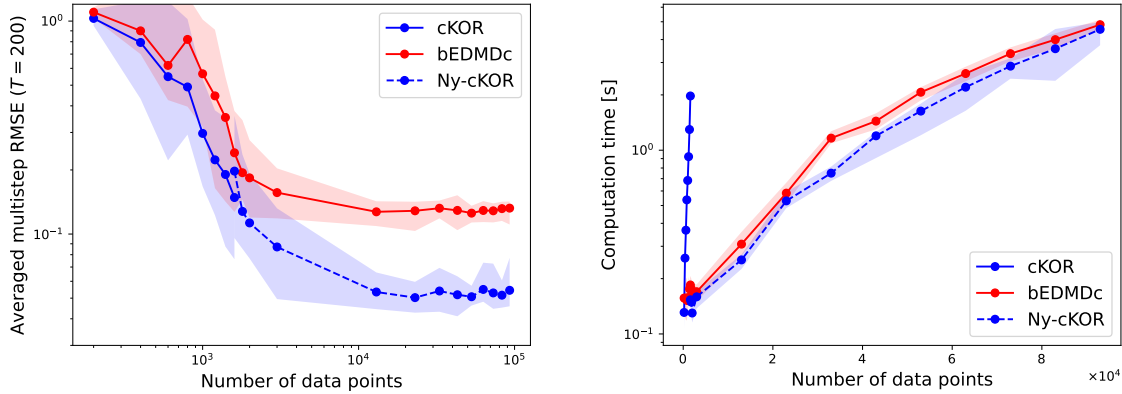


Figure 1: Comparing Koopman models based on cKOR, Ny-cKOR and the bEDMDc for various choices of the kernel width μ when $n_z = N$ and $n_z = m$, where n_z denotes the order of the lifted models. Comparison is provided in terms of the averaged RMSE of the 1-step-ahead prediction of the models over the test set.

Figure 1a confirms the enhanced accuracy of our nonparametric cKOR estimator as it reaches a significantly lower error than bEDMDc across μ values – showing a greater hyperparameter range of increased accuracy. Additionally, when lowering the regularization⁸, our cKOR estimator’s accuracy increases, achieving up to an order of magnitude better accuracy than bEDMDc. Even when we reduce complexity by projecting on a subset of data for our sketched Ny-cKOR estimator, a similar but reduced advantage can be observed in Figure 1b.

Convergence & time-complexity. In the second experiment, the training data is varied in terms of the number of available trajectories, i.e., the trajectory time is fixed to 2.0 sec ($N = 200$ samples). The initial conditions of these trajectories are from a square and equidistant grid, while the inputs and the remaining initial conditions are uniformly randomly generated within the limits $|x_1|, |x_2| \leq 2$ and $|u| \leq 2$. The test data consists of 20 trajectories of length 2.0 sec ($T_{\text{test}} = 200$ samples) with the same initial condition generation, but driven by an input sequence of $u_t = 2 \sin(10\pi t)$. Both datasets are normalized with the state and input normalization factors: 3 and 2, respectively. All the approaches use the Gaussian kernel (8.2) to construct the lifted states with hyperparameter $\mu = 0.25$ and a regularization parameter of 10^{-7} . These values are empirically determined as “optimal” for the prediction RMSE and choosing the same settings allows for a fair comparison between cKOR, Ny-cKOR and bEDMDc. Note that, the bEDMDc approach takes the inducing points as centres, which are 200 uniformly randomly sampled points from the training dataset. Figure 2a illustrates the RMSE of the T_{test} -step-ahead prediction (8.3) averaged over the test trajectories versus the number of training datapoints. The solid lines represent the average RMSE over 20 runs and the shaded area gives the variation of the RMSE per run. For each run, a new training data

⁸See Appendix D, Figure 8b.



(a) Multistep RMSE over increasing training data. (b) Computation time over increasing training data.

Figure 2: Comparing RMSE of the T_{test} -step-head prediction performance of the models and computation time of their estimation over increasing training data. Our Ny-cKOR estimator attains significantly lower prediction errors with a generally lower complexity than bEDMDc.

set and inducing points are generated to provide statistically relevant results. Figure 2b shows the computation times, i.e., the estimation time of \mathbf{A}^\top , $\{\mathbf{B}^\top\}_{j=1}^{n_u}$ and \mathbf{C}^\top along with the n -step-ahead prediction/rollout time. Strikingly, both the average RMSE of cKOR and Ny-cKOR stays below of bEDMDc, confirming the inherent advantages of estimators derived using a nonparametric paradigm. This also illustrates the common bottleneck of full KRR estimators well over the number of datapoints, since the full cKOR scales with $\mathcal{O}(N^3)$, compared to bEDMDc with $\mathcal{O}((n_z(n_u + 1))^3)$ and Ny-cKOR $\mathcal{O}(m^3)$.

In line with our expectation, Ny-cKOR continues the trend of cKOR for larger datasets, as the computation time becomes intractable for the full cKOR estimator. For a single input, the bEDMDc complexity is comparable to Ny-cKOR, however it is important to stress that Ny-cKOR is substantially more computationally efficient than bEDMDc for higher input dimensions – by a factor of $(n_u + 1)^3$ – as it does not require taking a tensor product of features and inputs.

8.2. High-dimensional dataset: Kalman vortex street. Tackling high-dimensional systems in a parametric manner, often comes with challenges as the suitable basis for representation is of critical importance. Through this simulation study, we want to showcase the superiority of our nonparametric learning paradigm even when it is based on a fraction of the data points, which is highly important for scalability.

Figure 3 schematically illustrates the considered nonlinear system which generates a flow as a result of transverse non-slip movement of an oscillating cylinder as input. This flow exhibits vortex shedding causing vortex-induced vibrations on the structure, which accelerate material fatigue and may lead to failure [5]. In [24], the considered system is created and simulated using the Computational Fluid Dynamics (CFD) environment OpenFOAM. For the data generation, we refer to [24]. The system identification procedure is performed with

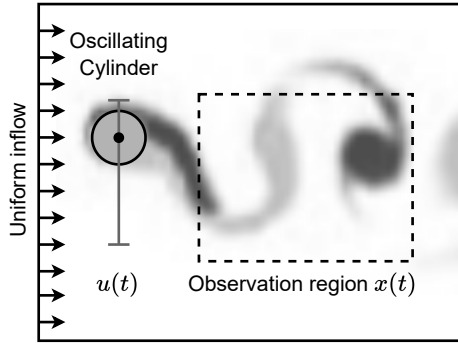


Figure 3: Schematic depiction of an oscillating cylinder submerged in a uniform flow.

the same setting as in [6]. For completeness, these settings are repeated here: the pressure, horizontal velocity and vertical velocity are observed in rectangular wake region of 41×45 , this amounts to a high state dimension of $n_x = 5535$. The flow conditions correspond to a Reynolds number of 100 and a Strouhal number of 0.167. The dataset consists of 11 timeseries of length $T = 1520$, with samples measured at 50Hz. These 11 timeseries correspond to 11 input sequences with a swept-sine input profile with different amplitudes and cylinder diameter ratios: $\{0.5, 0.75, \dots, 3.0\}$ that ends with a zero input. The timeseries are randomly split into 6 for training 3 for validation and 2 for testing. For statistically significant comparison, we assess the prediction performance of the methods on the test data over 20 randomly assigned splits. The training, validation and test datasets are normalized to constrain the states and inputs to values smaller than or equal to one.

For a fair comparison, all approaches use the same 400 inducing points for learning, meaning bEDMDc uses 400 RBF centres based on the inducing points of Ny-cKOR (and r -Ny-cKOR). Also all models are fitted using a hyperparameter and regularizer grid search on the validation data with the grids $\mu \in \{0.1, 0.5, 1, 10, 20, \dots, 60, 150, 175, \dots, 400\}$ and $\gamma \in N \times \{10^{-11}, 10^{-10}, \dots, 10^{-6}\}$ for the multi-step ($T_{\text{valid}} = 100$) state prediction RMSE. The rank r of the POD reduction is obtained after setting $\tau = 99.99\%$ in (6.4).

Table 3: Comparison of test prediction error for the estimated models on the actuated Karman vortex street over in terms of the averaged mean NRMSE for multi-step prediction of length $T_{\text{test}} = 3T_{\text{valid}}$ over 20 random test-validation-train splits.

	Ny-cKOR	r -Ny-cKOR	bEDMDc
test NRMSE	0.1572 ± 0.0489	0.2063 ± 0.1088	0.4106 ± 0.9765

As shown in Table 3, on average, both models from r -Ny-cKOR and Ny-cKOR significantly outperform those of bEDMDc. Strikingly, the error variance compared to bEDMDc for our Ny-cKOR and r -Ny-cKOR models is $20\times$ and $10\times$ smaller, respectively. Figure 4 shows an examples of the significant performance loss due to the large error variance of bEDMDc models. By just comparing the flow plots, it becomes clear that bEDMDc quickly deteriorates and does not resemble any aspect of the flow, as opposed to Ny-cKOR which stays quite accurate over

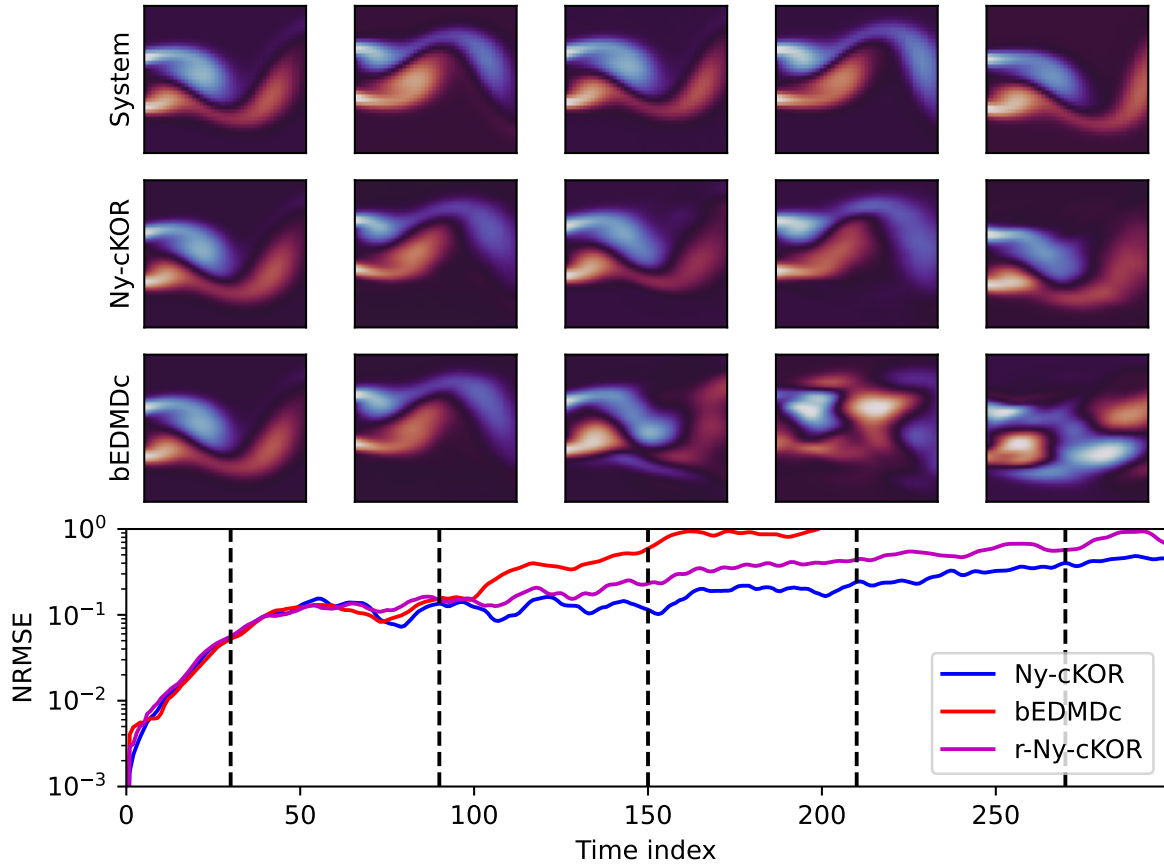


Figure 4: A prediction of the flow observation region showing the significant implications of reduced prediction error variance for Ny-cKOR models, leading to higher fidelity models.

the entire horizon. The reduced model of r -Ny-cKOR comes with an offset to Ny-cKOR but does not exhibit the performance loss of bEDMDc.

This example clearly demonstrates order-of-magnitude better performance of our (r -)Ny-cKOR models for an unknown high-dimensional control system, confirming our hypothesis that parametric paradigms quickly reach their limits for large-scale systems.

8.3. Model predictive control: Damped duffing oscillator. Next we investigate predictive control of the Duffing oscillator (8.1) of Section 8.1. The autonomous part $\mathbf{f}(\mathbf{x})$ has two stable equilibrium points while the origin is unstable. The vector field of the system is plotted in Figure 5a to illustrate if the control trajectories leverage the dynamics to gain performance. In this example, the Koopman MPC approach of Section 7, the iterative LPV-MPC approach based on a *standard LPV model* (non-exact conversion) of (8.1), a LTI MPC based on a linearized model of (8.1) are compared. The nonlinear MPC (NMPC) solution with the exact nonlinear model of (8.1) is considered as *the ground truth*.

The initial condition of the simulated scenario is set to $[1 \ 1]^\top$ and the state reference consists of the two equilibria: $[-1, 0]^\top$ and $[0, 0]^\top$, for 9s and 3s, respectively. The weighting

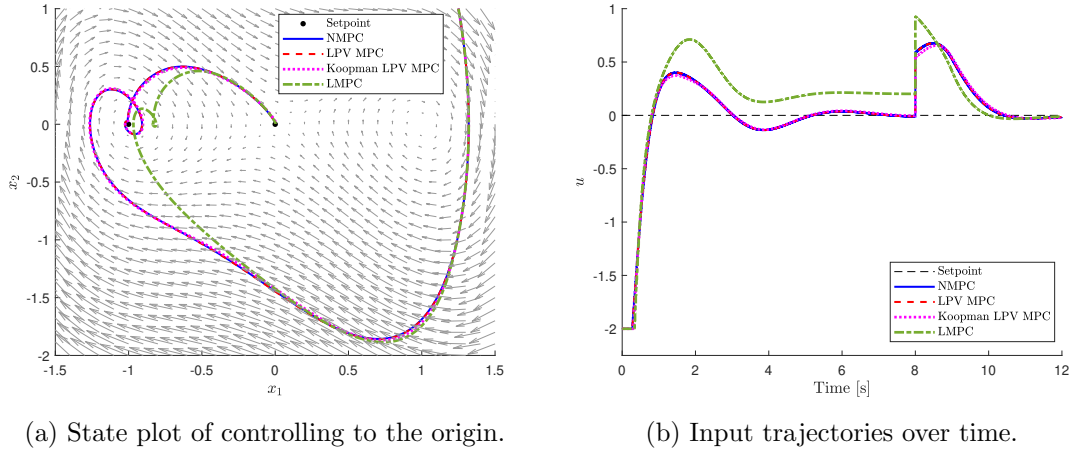


Figure 5: Comparing the resulting trajectories of the MPC approaches.

matrices are chosen as $\mathbf{Q} = \text{diag}(6, 1)$, $R = 5$ and $\mathbf{Q}_T = 100\mathbf{Q}$. The horizon is set to 100 steps, i.e. $T = 100$ with a sampling time of $\Delta_t = 0.01s$. Lastly, the constraints are sets as $-2 \leq u \leq 2$, $-3 \leq x_1 \leq 3$ and $-3 \leq x_2 \leq 3$. These settings are such chosen such that the knowing accurate nonlinear system behaviour is rewarded and that the desired setpoints are reached.

The linear MPC (LMPC) model is obtained by linearizing the system equations around the origin. LPV LMPC linearizes the system equations around the prior predicted states and optimized inputs and its initial guess is the initial condition over the horizon and zero inputs. The same initial guess is used for NMPC, which also has access to the system equations. Koopman LPV-MPC does not have access to the system equations, instead it uses training data ($N = 704$) in a state domain of $-2 \leq x_1 \leq 2$ and $-2 \leq x_2 \leq 2$ and an input domain of $[-2, 2]$. The bilinear model is constructed via r -Ny-cKOR with 100 uniformly randomly sampled inducing points, $r = 29$ and a hyperparameter grid search over validation data.

From Figures 5a and 5a, it can be observed that Koopman LPV-MPC, LPV LMPC and NMPC are almost identical, while they showcase a clear performance improvement compared to LMPC. Specifically, LMPC requires extra input effort between 1s and 3s, because around $x_1 = -0.2$ and $x_2 = -1.25$, the LMPC solution goes against the vector field. The other approaches use the vector field to reach the setpoint and thus requiring less input. In addition, there is a large offset between the settled state of LMPC and the setpoint, which then leads to an additional input effort to stabilize in the origin. The other approaches are almost identical, which implies that (1) the system and/or control task is not challenging enough and that (2) the bilinear Koopman model accurately identifies the nonlinear system.

8.4. Making data collection hard: Unstable system with linearly uncontrollable origin.

For the next example, the following Van der Pol oscillator

$$(8.4) \quad \dot{\mathbf{x}} = \begin{bmatrix} x_2 \\ -x_1 - \frac{1}{2}x_2(1 - x_1^2) \end{bmatrix} + \begin{bmatrix} 0 \\ x_1 u \end{bmatrix},$$

where the state is measured with sampling time $\Delta_t = 0.05s$ and the input is actuated in a synchronised ZOH manner. This is an interesting example for three reasons: the origin is linearly uncontrollable, the optimal solution to drive the system from arbitrary initial condition to the origin is known, and the system offers simple analysis because it is planar. The optimal unconstrained solution for the cost function

$$(8.5) \quad J(\mathbf{x}, u) = x_2^2 + u^2$$

is the feedback law: $u = -x_1x_2$ [66]. Thus the control task is to regulate the system to the origin while minimizing the aforementioned cost function. In other words, this system can showcase the potential of nonlinear control techniques as opposed to controllers based on linear state-space models.

The control objective is to stabilize the system in the origin from initial conditions within the unstable limit cycle and with the cost function (8.5). Specifically, the initial conditions $[-2, -2]^\top$, $[-2, 2]^\top$, $[2, -2]^\top$ and $[2, 2]^\top$ are considered with $\mathbf{Q} = \text{diag}(0, 1)$, $\mathbf{Q}_T = \mathbf{Q}$ and $R = 1$. The horizon is chosen as the minimal one such that NMPC is able to stabilize in the origin. This resulted in a horizon of 100 steps, which is relatively big and thus another indicator of a difficult to control system. The latter in combination with being open-loop unstable in the considered region, complicates the data gathering step for determining the bilinear Koopman model. For the training and the validation data, the NMPC controller is used to control the system to the origin with an exploratory uniform random disturbance within interval $[-2, 2]$. The hyperparameter and regularization parameter are obtained by employing a grid search on the validation data. The same initialization of the scheduling is used as in the previous example.

Figure 6a shows the resulting control trajectories for NMPC and Koopman LPV-MPC. For these settings, the LPV LMPC and LMPC controllers fail to stabilize into the origin, due to linearization limitations and the linearly uncontrollable property. The latter clearly highlights an advantage for the Koopman LPV-MPC scheme. However, the control trajectories of Koopman LPV-MPC deviate from the trajectories of the NMPC with full exact model knowledge. The aforementioned deviations are quantified with RMSE (8.3): RMSE of Koopman LPV-MPC is $2.83 \cdot 10^{-1}$ and of NMPC: $1.01 \cdot 10^{-1}$. Due to its data-driven nature, the model is inherently approximate model, while the NMPC works with perfect system knowledge. The latter is illustrated in Figure 6b by requiring a higher input as opposed to following the vector field. This result is still significant, as we solve a single QP at every timestep and do not require any initial guess for the scheduling or employment of model-based planners.

9. Conclusion. In this work, we proposed a novel framework for learning Koopman operators for control-affine systems in RKHS that offers computation advantages and strong theoretical guarantees in terms of operator learning in RKHS. As a result, the regression problem is independent of the feature and input dimensionality and only discretized by the data.

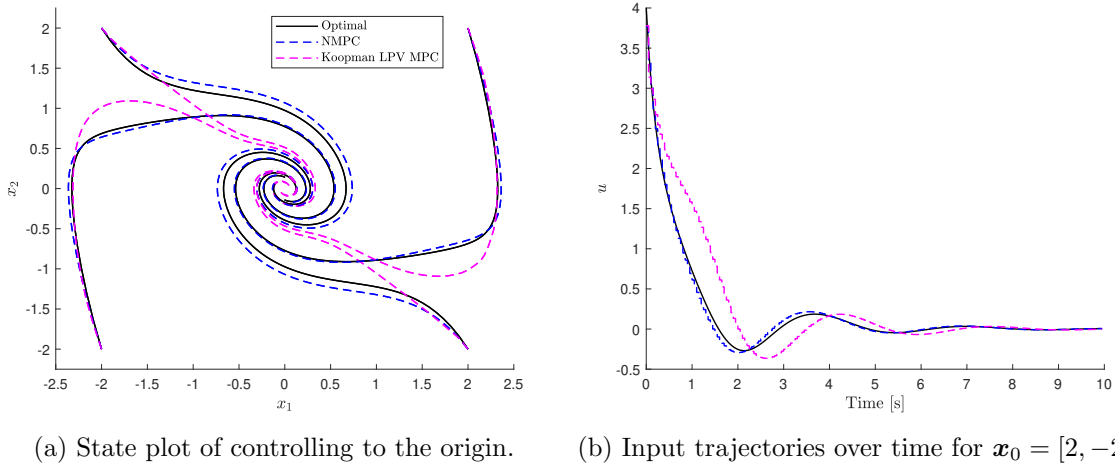


Figure 6: Comparing the resulting trajectories of the MPC approaches.

Furthermore, it delivers a bilinear Koopman-based model in a closed-form relying fully on a non-parametric representation of a control-affine system in an RKHS. The control-Koopman operator linearly evolves the lifted states given an initial condition and a sequence of control inputs.

We rigorously derive our representation for deterministic control systems that allows us to push the commonly considered input-dependence of Koopman operators entirely into its domain. Then, by leveraging the (operator) kernel trick, we derive end-to-end kernelized data-driven estimators for operator-theoretic control system modeling, a result missing from the literature. Due to this data-driven basis, our results present a significant advance in operator learning for systems with inputs. Namely, we provide an unifying framework as a direct analogue to the established autonomous case, including many Koopman-based state-space models (Table 2). Furthermore, our end-to-end application of the “kernel trick” through a nonparametric paradigm removes the need for meticulous dictionary selection that often relies on ad-hoc choices. We also derive closed-form expressions for operator learning using our non-parametric framework – including a variety of estimators – and use Nyström approximations (sketching) to make the KKR estimator applicable to large-scale problems. As a consequence, the computational complexity of our sketched estimator is only dependent on a small subset of the training data, i.e. $\mathcal{O}(m^3)$ with $m \ll N$, while the computational complexity of comparable estimators commonly scales with the number of features and input dimension as $\mathcal{O}((n_z(n_u + 1))^3)$.

Finally, we also demonstrate that our bilinear Koopman model offers an accurate and efficient linear multi-step predictor of the nonlinear system behaviour for a finite horizon, which is highly useful within a MPC scheme. As a result, the bilinear Koopman model is employed for control by interpreting it as an LPV model with known scheduling to make use of the LPV-MPC scheme. In order to reduce the complexity within this scheme, the

lifted state dimension of the estimated bilinear model is reduced using a truncated POD basis transformation. Such a reduction approach is handy for control design, because a small subset of the training data still results into relatively large lifted state dimensions. Yet, it offers one a similar multi-step prediction performance for a significant reduction of lifted states. To this end, employing our bilinear model for control lead to a comparable performance to NMPC, while offering more flexibility and a better performance compared to standard (LPV-)MPC based on ground-truth linearized models.

Acknowledgments. The authors thank Nicolas Hoischen for his feedback on the manuscript and Jan Decuyper for sharing the details of the Karman vortex example.

REFERENCES

- [1] T. E. AHMAD, L. BROGAT-MOTTE, P. LAFORGUE, AND F. D'ALCHÉ BUC, *Sketch in, sketch out: Accelerating both learning and inference for structured prediction with kernels*, 2023, <https://arxiv.org/abs/2302.10128>.
- [2] N. ARONSZAJN, *Theory of reproducing kernels*, Transactions of the American Mathematical Society, 68 (1950), p. 337, <https://doi.org/10.2307/1990404>, <https://www.jstor.org/stable/1990404?origin=crossref>.
- [3] O. AZENCOT, N. B. ERICHSOHN, V. LIN, AND M. MAHONEY, *Forecasting sequential data using consistent koopman autoencoders*, vol. 119, PMLR, 7 2020, pp. 475–485, <https://proceedings.mlr.press/v119/azencot20a.html>.
- [4] P. BATLLE, M. DARCY, B. HOSSEINI, AND H. OWHADI, *Kernel methods are competitive for operator learning*, Journal of Computational Physics, 496 (2024), p. 112549, <https://doi.org/https://doi.org/10.1016/j.jcp.2023.112549>, <https://www.sciencedirect.com/science/article/pii/S0021999123006447>.
- [5] P. W. BEARMAN, *Vortex shedding from oscillating bluff bodies*, Annual Review of Fluid Mechanics, 16 (1984), pp. 195–222, <https://doi.org/10.1146/annurev.fl.16.010184.001211>.
- [6] G. BEINTEMA, *Data-driven Learning of Nonlinear Dynamic Systems: A Deep Neural State-Space Approach*, phd thesis 1 (research tu/e / graduation tu/e), Electrical Engineering, Mar. 2024. Proefschrift.
- [7] T. BERRY, D. GIANNAKIS, AND J. HARLIM, *Nonparametric forecasting of low-dimensional dynamical systems*, Physical Review E, 91 (2015), p. 032915, <https://doi.org/10.1103/PhysRevE.91.032915>.
- [8] P. BEVANDA, M. BEIER, S. HESHMATI-ALAMDARI, S. SOSNOWSKI, AND S. HIRCHE, *Towards data-driven lqr with koopmanizing flows*, IFAC-PapersOnLine, 55 (2022), pp. 13–18, <https://doi.org/10.1016/j.ifacol.2022.07.601>.
- [9] P. BEVANDA, M. BEIER, A. LEDERER, S. SOSNOWSKI, E. HÜLLERMEIER, AND S. HIRCHE, *Koopman kernel regression*, in Advances in Neural Information Processing Systems, vol. 36, 2023, pp. 16207–16221, https://proceedings.neurips.cc/paper_files/paper/2023/file/34678d08b36076de986df95c5bbba92f-Paper-Conference.pdf.
- [10] P. BEVANDA, S. SOSNOWSKI, AND S. HIRCHE, *Koopman operator dynamical models: Learning, analysis and control*, Annual Reviews in Control, 52 (2021), pp. 197–212, <https://doi.org/https://doi.org/10.1016/j.arcontrol.2021.09.002>.
- [11] E. M. BOLLT, *Geometric considerations of a good dictionary for Koopman analysis of dynamical systems: Cardinality, “primary eigenfunction,” and efficient representation*, Communications in Nonlinear Science and Numerical Simulation, 100 (2021), <https://doi.org/10.1016/j.cnsns.2021.105833>.
- [12] D. BRUDER, X. FU, R. B. GILLESPIE, C. D. REMY, AND R. VASUDEVAN, *Data-driven control of soft robots using koopman operator theory*, IEEE Transactions on Robotics, 37 (2021), pp. 948–961, <https://doi.org/10.1109/TRO.2020.3038693>.
- [13] D. BRUDER, X. FU, AND R. VASUDEVAN, *Advantages of bilinear koopman realizations for the modeling and control of systems with unknown dynamics*, IEEE Robotics and Automation Letters, PP (2021), pp. 1–1, <https://doi.org/10.1109/LRA.2021.3068117>.
- [14] S. L. BRUNTON, M. BUDIŠIĆ, E. KAISER, AND J. N. KUTZ, *Modern koopman theory for dynamical*

- systems*, SIAM Review, 64 (2022), pp. 229–340, <https://doi.org/10.1137/21M1401243>.
- [15] M. BUDIŠIĆ, R. MOHR, AND I. MEZIĆ, *Applied koopmanism*, Chaos, 22 (2012), <https://doi.org/10.1063/1.4772195>.
- [16] E. CALDARELLI, A. CHATALIC, A. COLOMÉ, C. MOLINARI, C. OCAMPO-MARTINEZ, C. TORRAS, AND L. ROSASCO, *Linear quadratic control of nonlinear systems with koopman operator learning and the nyström method*, (2024), <http://arxiv.org/abs/2403.02811>.
- [17] A. CAPONNETTO AND E. D. VITO, *Optimal rates for the regularized least-squares algorithm*, Foundations of Computational Mathematics, 7 (2007), pp. 331–368, <https://doi.org/10.1007/s10208-006-0196-8>.
- [18] C. CARMELI, E. DE VITO, AND A. TOIGO, *Vector Valued Reproducing Kernel Hilbert Spaces of Integrable Functions and Mercer Theorem*, Analysis and Applications, 4 (2006), pp. 377–408.
- [19] C. CARMELI, E. DE VITO, A. TOIGO, AND V. UMANITÀ, *Vector Valued Reproducing Kernel Hilbert Spaces and Universality*, Analysis and Applications, 08 (2010), pp. 19–61, <https://doi.org/10.1142/S0219530510001503>.
- [20] A. CHATALIC, N. SCHREUDER, L. ROSASCO, AND A. RUDI, *Nyström kernel mean embeddings*, in Proceedings of the 39th International Conference on Machine Learning, vol. 162 of Proceedings of Machine Learning Research, PMLR, 17–23 Jul 2022, pp. 3006–3024.
- [21] A. CHATTERJEE, *An introduction to the proper orthogonal decomposition*, Current Science, 78 (2000), pp. 808–817, <http://www.jstor.org/stable/24103957> (accessed 2023-10-15).
- [22] P. CVITANOVIĆ, R. ARTUSO, R. MAINIERI, G. TANNER, AND G. VATTAY, *Chaos: Classical and Quantum*, Niels Bohr Inst., Copenhagen, 2016, <http://ChaosBook.org/>.
- [23] S. DAS AND D. GIANNAKIS, *Delay-coordinate maps and the spectra of koopman operators*, Journal of Statistical Physics, 175 (2019), pp. 1107–1145, <https://doi.org/10.1007/s10955-019-02272-w>.
- [24] J. DECUYPER, T. DE TROYER, K. TIELS, J. SCHOUKENS, AND M. RUNACRES, *A nonlinear model of vortex-induced forces on an oscillating cylinder in a fluid flow*, Journal of Fluids and Structures, 96 (2020), p. 103029, <https://doi.org/https://doi.org/10.1016/j.jfluidstructs.2020.103029>.
- [25] F. DIETRICH, T. N. THIEM, AND I. G. KEVREKIDIS, *On the koopman operator of algorithms*, SIAM Journal on Applied Dynamical Systems, 19 (2020), pp. 860–885, <https://doi.org/10.1137/19M1277059>.
- [26] A. S. DOGRA AND W. REDMAN, *Optimizing neural networks via koopman operator theory*, in Advances in Neural Information Processing Systems, H. Larochelle, M. Ranzato, R. Hadsell, M. Balcan, and H. Lin, eds., vol. 33, 2020, pp. 2087–2097, https://proceedings.neurips.cc/paper_files/paper/2020/file/169806bb68ccbf5e6f96ddc60c40a044-Paper.pdf.
- [27] A. DOMAHIDI AND J. JEREZ, *Forces professional*. Embotech AG, url=<https://embotech.com/FORCES-Pro>, 2014–2019.
- [28] K.-J. ENGEL AND R. NAGEL, *One-Parameter Semigroups for Linear Evolution Equations*, vol. 194, Springer-Verlag, 2000, <https://doi.org/10.1007/b97696>, <http://link.springer.com/10.1007/b97696>.
- [29] A. FALINI, *A review on the selection criteria for the truncated svd in data science applications*, Journal of Computational Mathematics and Data Science, 5 (2022), p. 100064, <https://doi.org/https://doi.org/10.1016/j.jcmds.2022.100064>.
- [30] D. GIANNAKIS, *Data-driven spectral decomposition and forecasting of ergodic dynamical systems*, Applied and Computational Harmonic Analysis, 47 (2019), pp. 338–396, <https://doi.org/10.1016/j.acha.2017.09.001>.
- [31] D. GIANNAKIS, J. SLAWINSKA, AND Z. ZHAO, *Spatiotemporal feature extraction with data-driven koopman operators*, in Proceedings of the 1st International Workshop on Feature Extraction: Modern Questions and Challenges at NIPS 2015, vol. 44 of Proceedings of Machine Learning Research, Montreal, Canada, 11 Dec 2015, PMLR, pp. 103–115, <https://proceedings.mlr.press/v44/giannakis15.html>.
- [32] D. GOSWAMI AND D. A. PALEY, *Global bilinearization and controllability of control-affine nonlinear systems: A koopman spectral approach*, in 2017 IEEE 56th Annual Conference on Decision and Control (CDC), 2017, pp. 6107–6112, <https://doi.org/10.1109/CDC.2017.8264582>.
- [33] D. GOSWAMI AND D. A. PALEY, *Bilinearization, reachability, and optimal control of control-affine nonlinear systems: A koopman spectral approach*, IEEE Transactions on Automatic Control, 67 (2022), pp. 2715–2728, <https://doi.org/10.1109/TAC.2021.3088802>.
- [34] Y. GUO, B. HOUSKA, AND M. E. VILLANUEVA, *A tutorial on pontryagin-koopman operators for infinite horizon optimal control*, in 2022 IEEE 61st Conference on Decision and Control (CDC), 2022, pp. 6800–6805, <https://doi.org/10.1109/CDC51059.2022.9992548>.

- [35] Y. GUO, M. KORDA, I. G. KEVREKIDIS, AND Q. LI, *Learning parametric koopman decompositions for prediction and control*, (2023), <http://arxiv.org/abs/2310.01124>.
- [36] D. A. HAGGERTY, M. J. BANKS, E. KAMENAR, A. B. CAO, P. C. CURTIS, I. MEZIĆ, AND E. W. HAWKES, *Control of soft robots with inertial dynamics*, *Science Robotics*, 8 (2023), <https://doi.org/10.1126/scirobotics.add6864>.
- [37] M. HASELI AND J. CORTÉS, *Modeling nonlinear control systems via koopman control family: Universal forms and subspace invariance proximity*, (2023), <http://arxiv.org/abs/2307.15368>.
- [38] J. H. HOEKSTRA, B. CSEPPENTÓ, G. I. BEINTEMA, M. SCHOUKENS, Z. KOLLÁR, AND R. TÓTH, *Computationally efficient predictive control based on ann state-space models*, 2023, <https://arxiv.org/abs/2303.17305>.
- [39] T. HOFMANN, B. SCHÖLKOPF, AND A. J. SMOLA, *Kernel methods in machine learning*, *The Annals of Statistics*, 36 (2008), <https://doi.org/10.1214/009053607000000677>.
- [40] B. HOUSKA, *Convex operator-theoretic methods in stochastic control*, (2023), <http://arxiv.org/abs/2305.17628>.
- [41] L. C. IACOB, M. SCHOUKENS, AND R. TÓTH, *Finite dimensional koopman form of polynomial nonlinear systems**, *IFAC-PapersOnLine*, 56 (2023), pp. 6423–6428, <https://doi.org/https://doi.org/10.1016/j.ifacol.2023.10.849>. 22nd IFAC World Congress.
- [42] L. C. IACOB, R. TÓTH, AND M. SCHOUKENS, *Koopman form of nonlinear systems with inputs*, *Automatica*, 162 (2024), p. 111525, <https://doi.org/https://doi.org/10.1016/j.automatica.2024.111525>.
- [43] INGO STEINWART AND ANDREAS CHRISTMANN, *Support Vector Machines*, *Information Science and Statistics*, Springer, New York, NY, first ed., 2008.
- [44] E. KAISER, J. N. KUTZ, AND S. L. BRUNTON, *Data-driven discovery of koopman eigenfunctions for control*, *Machine Learning: Science and Technology*, 2 (2021), p. 035023, <https://doi.org/10.1088/2632-2153/abf0f5>.
- [45] M. KHOSRAVI, *Representer theorem for learning koopman operators*, *IEEE Transactions on Automatic Control*, 68 (2023), pp. 2995–3010, <https://doi.org/10.1109/TAC.2023.3242325>.
- [46] S. KLUS, F. NÜSKE, AND S. PEITZ, *Koopman analysis of quantum systems**, *Journal of Physics A: Mathematical and Theoretical*, 55 (2022), p. 314002, <https://doi.org/10.1088/1751-8121/ac7d22>.
- [47] S. KLUS, I. SCHUSTER, AND K. MUANDET, *Eigendecompositions of transfer operators in reproducing kernel hilbert spaces*, *Journal of Nonlinear Science*, 30 (2020), pp. 283–315, <https://doi.org/10.1007/s00332-019-09574-z>.
- [48] B. O. KOOPMAN, *Hamiltonian systems and transformation in hilbert space.*, *Proceedings of the National Academy of Sciences of the United States of America*, 17 5 (1931), pp. 315–8.
- [49] M. KORDA AND I. MEZIĆ, *On convergence of extended dynamic mode decomposition to the koopman operator*, *Journal of Nonlinear Science*, 28 (2018), pp. 687–710, <https://doi.org/10.1007/s00332-017-9423-0>.
- [50] M. KORDA AND I. MEZIĆ, *Koopman Model Predictive Control of Nonlinear Dynamical Systems*, Springer International Publishing, 2020, pp. 235–255, https://doi.org/10.1007/978-3-030-35713-9_9.
- [51] M. KORDA AND I. MEZIĆ, *Linear predictors for nonlinear dynamical systems: Koopman operator meets model predictive control*, *Automatica*, 93 (2018), pp. 149–160, <https://doi.org/https://doi.org/10.1016/j.automatica.2018.03.046>.
- [52] M. KORDA AND I. MEZIĆ, *Optimal construction of koopman eigenfunctions for prediction and control*, *IEEE Transactions on Automatic Control*, 65 (2020), pp. 5114–5129, <https://doi.org/10.1109/TAC.2020.2978039>.
- [53] V. KOSTIC, K. LOUNICI, P. NOVELLI, AND M. PONTIL, *Sharp spectral rates for koopman operator learning*, in *Advances in Neural Information Processing Systems*, vol. 36, 2023, pp. 32328–32339.
- [54] V. KOSTIC, P. NOVELLI, A. MAURER, C. CILIBERTO, L. ROSASCO, AND M. PONTIL, *Learning dynamical systems via koopman operator regression in reproducing kernel hilbert spaces*, in *Advances in Neural Information Processing Systems*, vol. 35, 2022, pp. 4017–4031.
- [55] M. KRSTIC, *Forward-Complete Systems*, Birkhäuser Boston, Boston, 2009, pp. 171–190, https://doi.org/10.1007/978-0-8176-4877-0_11, https://doi.org/10.1007/978-0-8176-4877-0_11.
- [56] K. KÜSTER, *The Koopman Linearization of Dynamical Systems*, 2015, <https://homepages.laas.fr/henrion/mfol6/kari-kuester.pdf>.
- [57] Q. LI, F. DIETRICH, E. M. BOLLT, AND I. G. KEVREKIDIS, *Extended dynamic mode decomposition with dictionary learning: A data-driven adaptive spectral decomposition of the koopman operator*, *Chaos*:

- An Interdisciplinary Journal of Nonlinear Science, 27 (2017), p. 103111, <https://doi.org/10.1063/1.4993854>, <https://doi.org/10.1063/1.4993854>.
- [58] Z. LIU, N. OZAY, AND E. D. SONTAG, *On the non-existence of immersions for systems with multiple omega-limit sets*, IFAC-PapersOnLine, 56 (2023), pp. 60–64, <https://doi.org/https://doi.org/10.1016/j.ifacol.2023.10.1408>. 22nd IFAC World Congress.
- [59] G. MEANTI, A. CHATALIC, V. KOSTIC, P. NOVELLI, M. PONTIL, AND L. ROSASCO, *Estimating koopman operators with sketching to provably learn large scale dynamical systems*, in Advances in Neural Information Processing Systems, vol. 36, 2023, pp. 77242–77276.
- [60] F. MERRIKH-BAYAT AND M. AFSHAR, *Formulation of nonlinear control problems with actuator saturation as linear programs*, European Journal of Control, 61 (2021), pp. 133–141, <https://doi.org/https://doi.org/10.1016/j.ejcon.2021.07.005>, <https://www.sciencedirect.com/science/article/pii/S0947358021000960>.
- [61] I. MEZIC, *Spectral properties of dynamical systems, model reduction and decompositions*, Nonlinear Dynamics, 41 (2005), pp. 309–325, <https://doi.org/10.1007/s11071-005-2824-x>.
- [62] I. MEZIĆ, *Spectrum of the Koopman Operator, Spectral Expansions in Functional Spaces, and State-Space Geometry*, Journal of Nonlinear Science, 30 (2020), pp. 2091–2145.
- [63] I. MEZIĆ AND A. BANASZUK, *Comparison of systems with complex behavior*, Physica D: Nonlinear Phenomena, 197 (2004), pp. 101–133, <https://doi.org/https://doi.org/10.1016/j.physd.2004.06.015>, <https://www.sciencedirect.com/science/article/pii/S0167278904002507>.
- [64] M. MOLLENHAUER AND P. KOLTAI, *Nonparametric approximation of conditional expectation operators*, (2020), <http://arxiv.org/abs/2012.12917>.
- [65] M. MOLLENHAUER, N. MÜCKE, AND T. J. SULLIVAN, *Learning linear operators: Infinite-dimensional regression as a well-behaved non-compact inverse problem*, (2022), <http://arxiv.org/abs/2211.08875>.
- [66] V. NEVISTIC AND J. A. PRIMBS, *Constrained nonlinear optimal control: a converse hjb approach*, 1996.
- [67] H. NIJMEIJER AND A. J. VAN DER SCHAFT, *Nonlinear Dynamic Control Systems*, Springer, 1996.
- [68] F. NÜSKE AND S. KLUS, *Efficient approximation of molecular kinetics using random Fourier features*, The Journal of Chemical Physics, 159 (2023), p. 074105.
- [69] F. NÜSKE, S. PEITZ, F. PHILIPP, M. SCHALLER, AND K. WORTHMANN, *Finite-data error bounds for koopman-based prediction and control*, Journal of Nonlinear Science, 33 (2023), p. 14.
- [70] S. E. OTTO, G. R. MACCHIO, AND C. W. ROWLEY, *Learning nonlinear projections for reduced-order modeling of dynamical systems using constrained autoencoders*, Chaos: An Interdisciplinary Journal of Nonlinear Science, 33 (2023), <https://doi.org/10.1063/5.0169688>.
- [71] S. E. OTTO, S. PEITZ, AND C. W. ROWLEY, *Learning bilinear models of actuated koopman generators from partially-observed trajectories*, 2023, <https://arxiv.org/abs/2209.09977>.
- [72] S. E. OTTO AND C. W. ROWLEY, *Linearly recurrent autoencoder networks for learning dynamics*, SIAM Journal on Applied Dynamical Systems, 18 (2019), pp. 558–593, <https://doi.org/10.1137/18M1177846>.
- [73] S. E. OTTO AND C. W. ROWLEY, *Koopman operators for estimation and control of dynamical systems*, Annual Review of Control, Robotics, and Autonomous Systems, 4 (2021), pp. 59–87, <https://doi.org/10.1146/annurev-control-071020-010108>.
- [74] S. PAN AND K. DURAISAMY, *Physics-informed probabilistic learning of linear embeddings of nonlinear dynamics with guaranteed stability*, SIAM Journal on Applied Dynamical Systems, 19 (2020), pp. 480–509, <https://doi.org/10.1137/19M1267246>.
- [75] S. PEITZ AND S. KLUS, *Koopman operator-based model reduction for switched-system control of pdes*, Automatica, 106 (2019), pp. 184–191, <https://doi.org/10.1016/j.automatica.2019.05.016>.
- [76] S. PEITZ, S. OTTO, AND C. ROWLEY, *Data-driven model predictive control using interpolated koopman generators*, SIAM Journal on Applied Dynamical Systems, 19 (2020), p. 2162–2193, <https://doi.org/10.1137/20M1325678>.
- [77] F. PHILIPP, M. SCHALLER, K. WORTHMANN, S. PEITZ, AND F. NÜSKE, *Error analysis of kernel edmd for prediction and control in the koopman framework*, (2023), <http://arxiv.org/abs/2312.10460>.
- [78] J. PROCTOR, S. BRUNTON, AND J. KUTZ, *Generalizing koopman theory to allow for inputs and control*, SIAM Journal on Applied Dynamical Systems, 17 (2016), <https://doi.org/10.1137/16M1062296>.
- [79] J. L. PROCTOR, S. L. BRUNTON, AND J. N. KUTZ, *Dynamic mode decomposition with control*, 2014, <https://arxiv.org/abs/1409.6358>.

- [80] J. L. PROCTOR, S. L. BRUNTON, AND J. N. KUTZ, *Generalizing koopman theory to allow for inputs and control*, SIAM Journal on Applied Dynamical Systems, 17 (2018), pp. 909–930, <https://doi.org/10.1137/16M1062296>.
- [81] A. RAHIMI AND B. RECHT, *Random features for large-scale kernel machines*, in Advances in Neural Information Processing Systems, J. Platt, D. Koller, Y. Singer, and S. Roweis, eds., vol. 20, 2007, https://proceedings.neurips.cc/paper_files/paper/2007/file/013a006f03dbc5392effeb8f18fda755-Paper.pdf.
- [82] Y. RONG, Y. LIU, L. LU, W. WANG, AND D. MENG, *Divide-and-conquer learning with nystrom: Optimal rate and algorithm*, Proceedings of the AAAI Conference on Artificial Intelligence, 34 (2020), pp. 6696–6703, <https://doi.org/10.1609/aaai.v34i04.6147>.
- [83] M. SCHALLER, K. WORTHMANN, F. PHILIPP, S. PEITZ, AND F. NÜSKE, *Towards reliable data-based optimal and predictive control using extended dmd*, (2022), <http://arxiv.org/abs/2202.09084>.
- [84] P. SCHMID, K. E. MEYER, AND O. PUST, *Dynamic mode decomposition and proper orthogonal decomposition of flow in a lid-driven cylindrical cavity*, (2009).
- [85] P. J. SCHMID, *Dynamic mode decomposition of numerical and experimental data*, Journal of Fluid Mechanics, 656 (2010), p. 5–28, <https://doi.org/10.1017/S0022112010001217>.
- [86] L. SONG, J. HUANG, A. SMOLA, AND K. FUKUMIZU, *Hilbert space embeddings of conditional distributions with applications to dynamical systems*, in Proceedings of the 26th Annual International Conference on Machine Learning, ICML '09, New York, NY, USA, 2009, Association for Computing Machinery, p. 961–968, <https://doi.org/10.1145/1553374.1553497>, <https://doi.org/10.1145/1553374.1553497>.
- [87] R. STRÄSSER, J. BERBERICH, AND F. ALLGÖWER, *Robust data-driven control for nonlinear systems using the koopman operator**, IFAC-PapersOnLine, 56 (2023), pp. 2257–2262, <https://doi.org/https://doi.org/10.1016/j.ifacol.2023.10.1190>. 22nd IFAC World Congress.
- [88] J. A. TROPP, A. YURTSEVER, M. UDELL, AND V. CEVHER, *Practical sketching algorithms for low-rank matrix approximation*, SIAM Journal on Matrix Analysis and Applications, 38 (2017), pp. 1454–1485, <https://doi.org/10.1137/17M1111590>.
- [89] G. TURRI, V. KOSTIC, P. NOVELLI, AND M. PONTIL, *A randomized algorithm to solve reduced rank operator regression*, (2023).
- [90] M. E. VILLANUEVA, C. N. JONES, AND B. HOUSKA, *Towards global optimal control via koopman lifts*, Automatica, 132 (2021), p. 109610, <https://doi.org/10.1016/j.automatica.2021.109610>.
- [91] C. WILLIAMS AND M. SEEGER, *The effect of the input density distribution on kernel-based classifiers*, in ICML '00 Proceedings of the Seventeenth International Conference on Machine Learning, 2000, pp. 1159–1166.
- [92] C. WILLIAMS AND M. SEEGER, *Using the nystrom method to speed up kernel machines*, in Advances in Neural Information Processing Systems, vol. 13, 2000.
- [93] M. O. WILLIAMS, M. S. HEMATI, S. T. DAWSON, I. G. KEVREKIDIS, AND C. W. ROWLEY, *Extending data-driven koopman analysis to actuated systems*, IFAC-PapersOnLine, 49 (2016), pp. 704–709, <https://doi.org/10.1016/j.ifacol.2016.10.248>.
- [94] M. O. WILLIAMS, C. W. ROWLEY, AND I. G. KEVREKIDIS, *A kernel-based approach to data-driven koopman spectral analysis*, 2014, <https://arxiv.org/abs/1411.2260>.
- [95] J. T. WILSON, V. BOROVITSKIY, A. TEREININ, P. MOSTOWSKY, AND M. P. DEISENROTH, *Pathwise conditioning of gaussian processes*, J. Mach. Learn. Res., 22 (2021).
- [96] H. WU, F. NÜSKE, F. PAUL, S. KLUS, P. KOLTAI, AND F. NOÉ, *Variational koopman models: Slow collective variables and molecular kinetics from short off-equilibrium simulations*, The Journal of Chemical Physics, 146 (2017), p. 154104, <https://doi.org/10.1063/1.4979344>.
- [97] A. ZANELLI, A. DOMAHIDI, J. JEREZ, AND M. MORARI, *Forces nlp: an efficient implementation of interior-point... methods for multistage nonlinear nonconvex programs*, International Journal of Control, (2017), pp. 1–17.
- [98] C. ZHANG AND E. ZUAZUA, *A quantitative analysis of Koopman operator methods for system identification and predictions*, Comptes Rendus. Mécanique, (2023), <https://doi.org/10.5802/crmeca.138>. Online first.

Appendix A. Deriving Control-Koopman Operator Estimators. The use of *sampling operators* $\hat{S}_{(\cdot)}$ is particularly handy in the analysis of the optimization objective (**ERM**) in

either its primal or (convex) dual form as they relate the spaces \mathcal{H}_U and \mathcal{H}_X to the empirical distribution of data.

Informally, one can identify sampling operators as objects consisting of features evaluated at data and composed in rows, so-called “feature/data matrices”

$$(A.1) \quad \widehat{S}_+ = \begin{pmatrix} - & k_{\mathbf{x}_+^{(1)}}^\top & - \\ & \vdots & \\ - & k_{\mathbf{x}_+^{(i)}}^\top & - \\ & \vdots & \\ - & k_{\mathbf{x}_+^{(N)}}^\top & - \end{pmatrix} \quad \widehat{S} = \begin{pmatrix} - & k_{\mathbf{x}^{(1)}}^\top & - \\ & \vdots & \\ - & k_{\mathbf{x}^{(i)}}^\top & - \\ & \vdots & \\ - & k_{\mathbf{x}^{(N)}}^\top & - \end{pmatrix} \quad \mathbf{U}_j = \begin{pmatrix} - & e_{u_j^{(1)}}^\top & - \\ & \vdots & \\ - & e_{u_j^{(i)}}^\top & - \\ & \vdots & \\ - & e_{u_j^{(N)}}^\top & - \end{pmatrix}$$

where $k_{\mathbf{x}_+^{(i)}}$ are canonical feature maps evaluated at data datapoints $\mathbf{x}^{(i)}$ and $e_{u_j^{(i)}} := e_i u_j^{(i)}$ with e_i the i -th unit vector in \mathcal{H}_X . Note that, technically, for universal (infinite-dimensional) kernels, the above are not matrices but row vectors in $(\mathcal{H}_X)^N$. Also, the exact counterparts they empirically estimate – injection operators – are fully infinite-dimensional for universal kernels $S \in \text{HS}(\mathcal{H}_X, L^2)$. The key thing we will utilize in this derivation is the “kernel trick”, that allows us to work with the above row vectors in $(\mathcal{H}_X)^N$ without a loss of precision using Gram matrices, i.e. $\mathbf{K} = \widehat{S}\widehat{S}^\top$, that stay finite-dimensional ($N \times N$) even if \mathcal{H}_X is infinite-dimensional.

The sampling operators for the control-affected domain $\widehat{S}_U: \mathcal{H}_U \rightarrow \mathbb{R}^N$, autonomous $\widehat{S}: \mathcal{H}_X \rightarrow \mathbb{R}^N$ and target $\widehat{S}_+: \mathcal{H}_X \rightarrow \mathbb{R}^N$ are defined, respectively, as

$$\begin{aligned} \widehat{S}_U h &:= \frac{1}{\sqrt{N}} [\langle g, k_{\mathbf{x}_+^{(i)}} + \sum_{k \in n_u} k_{\mathbf{x}_+^{(i)}} u_k^{(i)} \rangle_{\mathcal{H}_X}]_{i \in [N]}, & \widehat{S}_+ g &:= \frac{1}{\sqrt{N}} [\langle g, k_{\mathbf{x}_+^{(i)}} \rangle_{\mathcal{H}_X}]_{i \in [N]}, \\ &= (\widehat{S} + \sum_{k \in n_u} \mathbf{U}_k \widehat{S}) g & \forall h \in \mathcal{H}_U, g \in \mathcal{H}_X. \end{aligned}$$

It is readily verified that their adjoints are given by

$$\begin{aligned} \widehat{S}_U^\top \mathbf{v} &= \frac{1}{\sqrt{N}} \sum_{i \in [N]} w_i k_{\mathbf{x}_+^{(i)}} + \sum_{k \in n_u} \frac{1}{\sqrt{N}} \sum_{i \in [N]} w_i k_{\mathbf{x}_+^{(i)}} u_k^{(i)}, & \widehat{S}_+^\top \mathbf{w} &= \frac{1}{\sqrt{N}} \sum_{i \in [N]} w_i k_{\mathbf{x}_+^{(i)}}, \\ &= (\widehat{S}^\top + \sum_{k \in n_u} \widehat{S}^\top \mathbf{U}_k^\top) \mathbf{w} & \forall \mathbf{v}, \mathbf{w} \in \mathbb{R}^N. \end{aligned}$$

By composing sampling operators using control affinity from Theorem 3.5, one obtains

$$\begin{aligned} C &:= \widehat{S}_U^\top \widehat{S}_U = \frac{1}{N} \sum_{i \in [N]} k_{\mathbf{x}^{(i)}, \mathbf{u}^{(i)}} \otimes k_{\mathbf{x}^{(i)}, \mathbf{u}^{(i)}}, & C_{++} &:= \widehat{S}_+^\top \widehat{S}_+ = \frac{1}{N} \sum_{i \in [N]} k_{\mathbf{x}_+^{(i)}} \otimes k_{\mathbf{x}_+^{(i)}}, \\ &\equiv \widehat{S}^\top \widehat{S} + \sum_{k \in n_u} \widehat{S}^\top \mathbf{U}_k^\top \mathbf{U}_k \widehat{S}, \end{aligned}$$

which are the input and target *covariance operators*, respectively, and

$$\begin{aligned} \mathbf{K}_U &:= \widehat{S}_U \widehat{S}_U^\top = \widehat{S} \widehat{S}^\top + \sum_{k \in n_u} \mathbf{U}_k \widehat{S} \widehat{S}^\top \mathbf{U}_k^\top, & \mathbf{K}_{++} &:= \widehat{S}_+ \widehat{S}_+^\top = N^{-1} [k(\mathbf{x}_+^{(i)}, \mathbf{x}_+^{(j)})]_{i, j \in [N]} \\ &= \mathbf{K} + \sum_{k \in n_u} \mathbf{U}_k \mathbf{K} \mathbf{U}_k^\top, \\ &= N^{-1} [k(\mathbf{x}^{(i)}, \mathbf{x}^{(j)}) + \sum_{k \in n_u} u_k^{(i)} k(\mathbf{x}^{(i)}, \mathbf{x}^{(j)}) u_k^{(j)}]_{i, j \in [N]}, \end{aligned}$$

the input and target *kernel matrices*, respectively. Moreover, the *target cross-covariance operators* $T^* : \mathcal{H}_X \rightarrow \mathcal{H}_U$, $T : \mathcal{H}_U \rightarrow \mathcal{H}_X$ are given by the formulas

$$\begin{aligned} T &:= \widehat{S}_U^\top \widehat{S}_+ = \frac{1}{N} \sum_{i \in [N]} k_{\mathbf{x}^{(i)}, \mathbf{u}^{(i)}} \otimes k_{\mathbf{x}_+^{(i)}} & T^* &:= \widehat{S}_+^\top \widehat{S}_U = \frac{1}{N} \sum_{i \in [N]} k_{\mathbf{x}_+^{(i)}} \otimes k_{\mathbf{x}^{(i)}, \mathbf{u}^{(i)}} \\ &= (\widehat{S}^\top + \sum_{k \in n_{\mathbf{u}}} \widehat{S}^\top \mathbf{U}_k^\top) \widehat{S}_+ & &= \widehat{S}_+^\top (\widehat{S} + \sum_{k \in n_{\mathbf{u}}} \mathbf{U}_k \widehat{S}). \end{aligned}$$

with time-shift cross-kernel matrices $\mathbf{K}_+^\top : \mathcal{H}_X \rightarrow \mathcal{H}_X$, $\mathbf{K}_+ : \mathcal{H}_X \rightarrow \mathcal{H}_X$

$$\mathbf{K}_+ = \mathcal{A}_{|\mathcal{T}|}(\mathbf{u}) \mathbf{K} := \widehat{S}_+ \widehat{S}^\top = N^{-1} [k(\mathbf{x}_+^{(i)}, \mathbf{x}^{(j)})]_{i,j \in [N]} \quad \mathbf{K}_+^\top := \widehat{S} \widehat{S}_+^\top = N^{-1} [k(\mathbf{x}^{(i)}, \mathbf{x}_+^{(j)})]_{i,j \in [N]}$$

We can then state the following result that follows the conventions from generic linear operator regression [89, Section 2].

Theorem A.1 (Control-Koopman Operator Estimators). *The control-Koopman operator restricted to the RKHS, can be empirically estimated by $\widehat{S}_U^\top \mathbf{W} \widehat{S}_+$, where $\mathbf{W} \in \mathbb{R}^{N \times N}$ follows⁹*

- (1) *from the Kernel Ridge Regression (KRR) algorithm $\widehat{\mathbf{G}}_\gamma$ minimizing (GERM) without rank constraint as*

$$\text{(KRR)} \quad \widehat{\mathbf{G}}_\gamma = \widehat{S}_U^\top \underbrace{(\mathbf{K}_U + \gamma \mathbf{I})^{-1}}_{\mathbf{W}} \widehat{S}_+,$$

defining the bilinear model for our objective (2.4a) via

$$\text{(A-KRR)} \quad \widehat{\mathbf{A}}_\gamma = \widehat{S}^\top (\mathbf{K}_U + \gamma \mathbf{I})^{-1} \widehat{S}_+ = (\mathbf{K}_U + \gamma \mathbf{I})^{-1} \mathbf{K}_+,$$

$$\text{(B-KRR)} \quad \widehat{\mathbf{B}}_{\gamma_k} = \widehat{S}^\top \mathbf{U}_k^\top (\mathbf{K}_U + \gamma \mathbf{I})^{-1} \widehat{S}_+ = \mathbf{U}_k^\top (\mathbf{K}_U + \gamma \mathbf{I})^{-1} \mathbf{K}_+;$$

- (2) *from the Reduced Rank Regression (RRR) algorithm minimizing (GERM) under a rank constraint $\widehat{\mathbf{G}} \in \{\text{HS}(\mathcal{H}_U, \mathcal{H}_X) \mid \text{rank}(\widehat{\mathbf{G}}) \leq r\}$ as*

$$\text{(RRR)} \quad \widehat{\mathbf{G}}_\gamma^{\text{RRR}} := C_\gamma^{-\frac{1}{2}} \llbracket C_\gamma^{-\frac{1}{2}} T \rrbracket_r = \widehat{S}_U^\top \underbrace{\mathbf{U}_r \mathbf{V}_r^\top}_{\mathbf{W}} \widehat{S}_+,$$

where $C_\gamma := C + \gamma \mathbf{I}$ is the Tikhonov-regularized input covariance with $\mathbf{V}_r = \mathbf{K}_U \mathbf{U}_r$ and $\mathbf{U}_r = [\mathbf{u}_1 \mid \dots \mid \mathbf{u}_r] \in \mathbb{R}^{N \times r}$ is such that (σ_i, \mathbf{u}_i) are the solution to the generalized eigenvalue problem

$$\text{(GEP)} \quad \mathbf{K}_{++} \mathbf{K}_U \mathbf{u}_i = \sigma_i^2 (\mathbf{K}_U + \gamma \mathbf{I}) \mathbf{u}_i, \text{ such that } \mathbf{u}_i^\top \mathbf{K}_U (\mathbf{K}_U + \gamma \mathbf{I}) \mathbf{u}_i = 1,$$

defining the bilinear model for our objective (2.4a) via

$$\text{(A-RRR)} \quad \widehat{\mathbf{A}}_\gamma^{\text{RRR}} = \widehat{S}^\top \mathbf{U}_r \mathbf{V}_r^\top \widehat{S}_+,$$

$$\text{(B-RRR)} \quad \widehat{\mathbf{B}}_{\gamma_k}^{\text{RRR}} = \mathbf{U}_k^\top \widehat{S}^\top \mathbf{U}_r \mathbf{V}_r^\top \widehat{S}_+;$$

⁹By Theorem 3.5, the above estimators are a composite sum of operators $\widehat{\mathbf{G}}_\gamma = \widehat{\mathbf{A}}_\gamma + \sum_{k \in n_{\mathbf{u}}} \widehat{\mathbf{B}}_{\gamma_k}$.

(3) from the Principal Component Regression (PCR) algorithm as

$$\text{(PCR)} \quad \widehat{\mathbf{G}}_\gamma^{\text{PCR}} := \llbracket \mathbf{C} \rrbracket_r^\dagger T = \widehat{\mathbf{S}}_U^\top \underbrace{\mathbf{U}_r \mathbf{V}_r^\top}_W \widehat{\mathbf{S}}_+,$$

where $\llbracket \mathbf{K}_U \rrbracket_r = \mathbf{V}_r \boldsymbol{\Sigma}_r \mathbf{V}_r^\top$ r -truncated SVD of \mathbf{K}_U , and $\mathbf{U}_r = \mathbf{V}_r \boldsymbol{\Sigma}_r^\dagger$ while $(\cdot)^\dagger$ denotes the Moore-Penrose pseudo-inverse, defining the bilinear model for our objective (2.4a) via

$$\text{(A-PCR)} \quad \widehat{\mathbf{A}}_\gamma^{\text{PCR}} = \widehat{\mathbf{S}}^\top \mathbf{U}_r \mathbf{V}_r^\top \widehat{\mathbf{S}}_+,$$

$$\text{(B-PCR)} \quad \widehat{\mathbf{B}}_{\gamma_k}^{\text{PCR}} = \mathbf{U}_k^\top \widehat{\mathbf{S}}^\top \mathbf{U}_r \mathbf{V}_r^\top \widehat{\mathbf{S}}_+;$$

Proof. After the use of control affinity of from Theorem 3.5 for the input sampling operators introduced previously, the results readily follow by a slight modification of results in [89, Proposition 2.1] and using [54, Proposition 4 & Theorem 4]. \blacksquare

Appendix B. State reconstruction: A cautionary tale.

The final step of the Koopman modelling procedure is to linearly reconstruct the original state from the lifted states. In general, two main methodologies are considered in the literature: a) fitting a matrix $\mathbf{C}^\top \in \mathbb{R}^{n_x \times N_z}$ that reconstructs the states using the following expression

$$\text{(B.1)} \quad \mathbf{x} = \mathbf{C}^\top \mathbf{z},$$

and b) adding the state \mathbf{x} to the observables/lifted states. In this way, \mathbf{C}^\top is expressed as

$$\text{(B.2)} \quad \mathbf{C}^\top = [\mathbf{I}_{n_x} \quad 0 \quad \cdots \quad 0]$$

For simplicity, we will consider the autonomous case here. Nevertheless, this transfers to the control-affine case as the lack of closure of the autonomous operator directly influences the control-affine operator as well, cf. Section 4.

The advantages of method two are that the reconstruction is predefined and the reconstruction error is zero. However, this comes at the cost of a restrictive assumption: the original state is part of the linearly evolving observables. Obviously, the original system is nonlinear in \mathbf{x} , which makes enforcing \mathbf{x} to be part of the linear observables a too restrictive assumption, especially whenever the original system has strong nonlinear behaviour in \mathbf{x} . In this case, the linear multi-step prediction performance deteriorates over time. For method a), \mathbf{C} can be simply be obtained by minimizing $\|\mathbf{X} - \mathbf{Z}\mathbf{C}\|_{\text{HS}}^2$ with the solution

$$\text{(B.3)} \quad \widehat{\mathbf{C}} = \mathbf{Z}^\dagger \mathbf{X}$$

where finite-dimensional sampling matrices \mathbf{X}, \mathbf{Z} (analogous to sampling operators) are

$$\text{(B.4)} \quad \mathbf{X}^\top = [\mathbf{x}^{(1)} \mid \cdots \mid \mathbf{x}^{(N)}] \in \mathbb{R}^{n_x \times N} \quad \mathbf{Z}^\top = [\mathbf{z}(\mathbf{x}^{(1)}) \mid \cdots \mid \mathbf{z}(\mathbf{x}^{(N)})] \in \mathbb{R}^{N_z \times N}.$$

This approach assumes that the reconstructed state lies within the span of the lifted states, which is a mild assumption on a compact set due to the low complexity of the identity mapping. The following remark and example showcase clear limitations of appending the state into the lifted states.

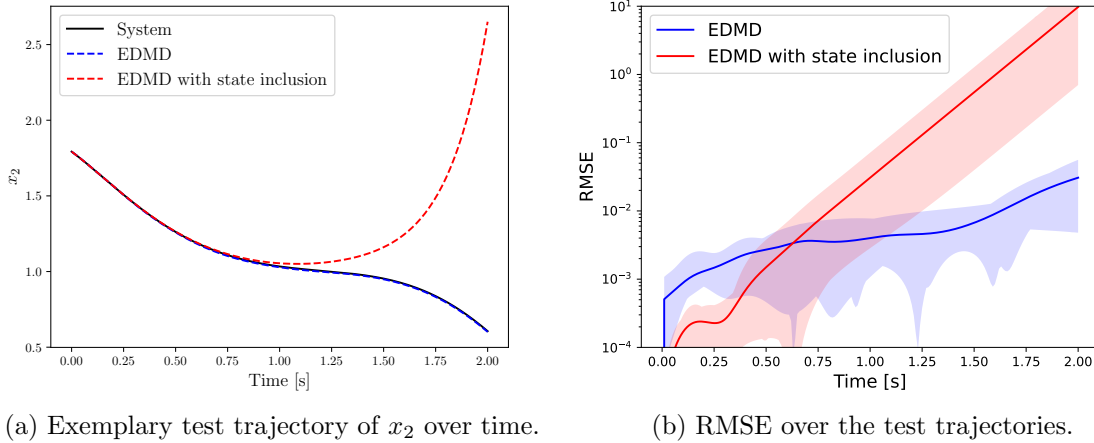


Figure 7: Comparison that demonstrates a clear multi-step prediction advantage for the nonparametric approach.

Remark B.1 (Theoretical issues of state inclusion). In case of appending the state to a feature map, existing work leaves the nonparametric setting. The universal RKHS that includes the state is $\mathcal{H}_{\text{id}} = \mathcal{H} \oplus \text{Id}(\mathbb{X})$ and is induced by the kernel $k_{\text{id}}(\mathbf{x}, \mathbf{x}') = k(\mathbf{x}, \mathbf{x}') + \mathbf{x}^\top \mathbf{x}'$. Existing literature that uses state-inclusion evaluates the empirical inner product that is only an approximation of the canonical one $k_{\text{id}}(\mathbf{x}, \mathbf{x}')$. Additionally, severe misspecification is incurred in a finite-data regime due to well-known closure-issues of state-inclusion. As Figure 7 shows, these effects are particularly severe for multiple fixed-points.

Experimental validation. The training dataset consists of 3000 datapoints from the Duffing oscillator (8.1) which are 300 trajectories of $T = 0.10s$, starting from a 17 by 17 equidistant grid of initial conditions within the limits $|x_1| \leq 2$ and $|x_2| \leq 2$ (the remaining initial conditions are uniformly randomly generated within these limits). The observables are Gaussian kernels (8.2) with all the states from the training data as centres. For state inclusion EDMD, the original state is added to these observables (to this end EDMD with state inclusion actually has two more lifted states). The validation dataset contains 60 trajectories of $T = 0.50s$, starting from uniformly randomly generated initial conditions within the aforementioned limits. Over this validation dataset, the hyperparameter and the regularization parameter γ are varied over $0.5, 1, 5, 10$ and $N \times \{10^{-11}, 10^{-10}, \dots, 10^{-5}\}$, respectively, with the RMSE (8.3) as performance measure. This grid search resulted in $\mu = 0.5$ and $\gamma = N \times 10^{-11}$ for both models. With these models, the prediction performance over time is compared on a test dataset, which consists of 10 trajectories with $T = 2.0s$, starting from uniformly randomly generated initial conditions within the aforementioned bounds. Figure 7a shows an exemplary test trajectory versus the predicted trajectories for the EDMD approaches over time. The entire forecast performance on the test data is depicted in Figure 7b, where the RMSE (8.3) is considered over the number trajectories where the shaded area represents the min-max over the data sets.

Both these figures clearly demonstrate the (relatively small) initial approximation advantage of state inclusion, due to the reconstruction error being zero. However, this advantage quickly diverges over time due to the closure problems of appending the states into observables.

Appendix C. Numerical implementation of the LPV-MPC.

To solve the optimization problem, a scheduling sequence is required to be determined, which should already be close to the state-trajectory of the optimal solution in order to ensure that the QP will provide an optimal solution for the underlying nonlinear predictive control problem. As we discussed it already, in the iterative LPV-MPC, the scheduling variables are iteratively updated using prior predicted lifted states, until \mathbf{U}_t converges. The prior predicted lifted states are the predicted lifted states that were computed in the previous iteration. Specifically, $\mathbf{p}_{0|t} = \mathbf{z}(\mathbf{x}_t)$ and $\mathbf{p}_{i|t} = \hat{\mathbf{z}}_{i|t}$ for $i = 1, 2, \dots, T-1$, where $\hat{\mathbf{z}}_{i|t}$ are the predicted lifted states in the previous iteration associated with the optimal input sequence found in that step. To start the iteration at time step t , the optimal input sequence \mathbf{U}_{t-1} associated predicted state sequence $\{\hat{\mathbf{z}}_{i|t-1}\}_{i=1}^T$ at time $t-1$, which was the result of converging iterations, is used as an initialisation. Specifically, $\mathbf{p}_{i|t} = \mathbf{z}_{i+1|t-1}$ for $i = 1, 2, \dots, T-1$ and $\mathbf{p}_{i|T-1} = \mathbf{z}_{T-1|t-1}$. This bootstrapping-based scheme provides an efficient way to kick start the iterations and provides fast convergence (in terms of a threshold) often no more than 2 or 3 steps. However, when the MPC is started at $t = 0$, no previous control cycle is present. For that case, the scheduling is initialized as a constant trajectory $\mathbf{p}_{i|t} = \mathbf{z}_{0|t}$ for $i = 1, 2, \dots, T-1$ and then the iterations are started. This typically results in a larger number of (7-10) iterations at the first time-instant when the MPC is switched on. To avoid the computational load of the iterative LPV-MPC scheme which comes from the repetitive solution of QPs in each control cycle, a simplification is the (simple) LPV-MPC scheme where the above described scheme is applied, but with only one iteration in each control cycle.

The optimization problem (7.3a) can be written as a single quadratic problem (note, the terms in the cost function independent of the input are dropped, since they are irrelevant for finding the optimal inputs) as shown below

$$(C.1) \quad \min_{\mathbf{U}_t} \quad \frac{1}{2} \mathbf{U}_t^T \mathbf{H} \mathbf{U}_t + \mathbf{h}^T \mathbf{U}_t$$

$$(C.2) \quad \text{s.t.} \quad \mathbf{L} \mathbf{U}_t \leq \mathbf{c} - \mathbf{M} \mathbf{z}(t) - \mathbf{D} \mathbf{x}_t,$$

with $\mathbf{H} \in \mathbb{R}^{n_u T \times n_u T}$ and $\mathbf{h} \in \mathbb{R}^{n_u T}$ defined as

$$(C.3) \quad \mathbf{H} = 2 (\mathbf{R} + \mathbf{\Gamma}^T(\mathbf{P}_t) \mathbf{C}^T \mathbf{Q} \mathbf{C} \mathbf{\Gamma}(\mathbf{P}_t))$$

$$(C.4) \quad \mathbf{h} = 2 (\mathbf{\Gamma}^T(\mathbf{P}_t) \mathbf{C}^T \mathbf{Q} (\mathbf{C} \mathbf{A} \mathbf{z}_{0|t} - \bar{\mathbf{X}}_t) - \mathbf{R} \bar{\mathbf{U}}_t),$$

where

$$(C.5) \quad \mathbf{P}_t = [\mathbf{p}_{0|t} \quad \mathbf{p}_{1|t} \quad \cdots \quad \mathbf{p}_{T-1|t}].$$

Similarly, $\bar{\mathbf{X}}_t$, $\bar{\mathbf{U}}_t$ with \mathbf{U}_t contain the state-, input reference and the inputs over the entire time horizon, respectively. The matrices $\mathbf{R} \in \mathbb{R}^{n_u T \times n_u T}$ and $\mathbf{Q} \in \mathbb{R}^{n_x T \times n_x T}$ concatenates weighting matrices over the diagonal: $\mathbf{R} = \text{diag}(\mathbf{R}, \dots, \mathbf{R})$ and $\mathbf{Q} = \text{diag}(\mathbf{Q}, \mathbf{Q}, \dots, \mathbf{Q}, \mathbf{Q}_T)$.

Next, we derive the inequality constraint expressions for \mathbf{L} , \mathbf{c} , \mathbf{M} and \mathbf{D} . The expressions for \mathbf{L} and \mathbf{c} in equation (C.2) are derived from the inequalities (7.3d) and (7.3e). The latter is rewritten as

$$(C.6) \quad \mathbf{W}_i \mathbf{x}_{i|t} + \mathbf{E}_i \mathbf{u}_{i|t} \leq \mathbf{b}_i, \quad \forall i = 1, 2, \dots, T$$

$$(C.7) \quad \mathbf{W}_T \mathbf{x}_{T|t} \leq \mathbf{b}_T$$

with

$$(C.8) \quad \mathbf{W}_i = \begin{bmatrix} 0 \\ 0 \\ -\mathbf{I}_{N_x} \\ \mathbf{I}_{N_x} \end{bmatrix}, \quad \mathbf{E}_i = \begin{bmatrix} -\mathbf{I}_{N_u} \\ \mathbf{I}_{N_u} \\ 0 \\ 0 \end{bmatrix}, \quad \mathbf{b}_i = \begin{bmatrix} -\mathbf{u}_{min} \\ \mathbf{u}_{max} \\ -\mathbf{x}_{min} \\ \mathbf{x}_{max} \end{bmatrix}, \quad \mathbf{W}_N = \begin{bmatrix} -\mathbf{I}_{N_x} \\ \mathbf{I}_{N_x} \end{bmatrix}, \quad \mathbf{b}_N = \begin{bmatrix} -\mathbf{x}_{min} \\ \mathbf{x}_{max} \end{bmatrix}$$

These constraints are stacked over the all the horizon steps to form

$$(C.9) \quad \mathbf{D} \mathbf{x}(t) + \mathbf{W} \mathbf{X}_t + \mathbf{E} \mathbf{U}_t \leq \mathbf{c}$$

where

$$(C.10) \quad \mathbf{D} = \begin{bmatrix} \mathbf{W}_0 \\ 0 \\ \vdots \\ 0 \end{bmatrix}, \quad \mathbf{W} = \begin{bmatrix} 0 & \cdots & 0 \\ \mathbf{W}_1 & \cdots & 0 \\ \vdots & \ddots & \vdots \\ 0 & \cdots & \mathbf{W}_N \end{bmatrix}, \quad \mathbf{E} = \begin{bmatrix} \mathbf{E}_0 & \cdots & 0 \\ \vdots & \ddots & \vdots \\ 0 & \cdots & \mathbf{E}_{N-1} \\ 0 & \cdots & 0 \end{bmatrix}, \quad \mathbf{c} = \begin{bmatrix} \mathbf{b}_0 \\ \mathbf{b}_1 \\ \vdots \\ \mathbf{b}_N \end{bmatrix}.$$

Equation (C.9) is rewritten, in terms of \mathbf{U}_t and $\mathbf{z}(t)$ by substituting the prediction model for \mathbf{X}_t , i.e. equations (C.13) and (C.14), as

$$(C.2) \quad \mathbf{L} \mathbf{U}_t \leq \mathbf{c} - \mathbf{M} \mathbf{z}(t) - \mathbf{D} \mathbf{x}(t),$$

with

$$(C.11) \quad \mathbf{L} = \mathbf{W} \mathbf{\Gamma}(\mathbf{P}_t) + \mathbf{E},$$

$$(C.12) \quad \mathbf{M} = \mathbf{W} \mathbf{A}.$$

The matrices \mathbf{A} and $\mathbf{\Gamma}$ originate from the following prediction model that predicts the future states over the horizon $\hat{\mathbf{Z}}_t$ given $\mathbf{z}_{0|t}$ and \mathbf{U}_t

$$(C.13) \quad \underbrace{\begin{bmatrix} \mathbf{z}_{1|t} \\ \mathbf{z}_{2|t} \\ \vdots \\ \mathbf{z}_{T|t} \end{bmatrix}}_{\hat{\mathbf{Z}}_t} = \underbrace{\begin{bmatrix} \mathbf{A}^\top \\ (\mathbf{A}^\top)^2 \\ \vdots \\ (\mathbf{A}^\top)^T \end{bmatrix}}_{\mathbf{A}} \mathbf{z}_{0|t} + \underbrace{\begin{bmatrix} \mathbf{B}(\mathbf{p}_{0|t}) & 0 & \cdots & 0 \\ \mathbf{A}^\top \mathbf{B}(\mathbf{p}_{0|t}) & \mathbf{B}(\mathbf{p}_{1|t}) & \cdots & 0 \\ \vdots & \vdots & \ddots & \vdots \\ (\mathbf{A}^\top)^{T-1} \mathbf{B}(\mathbf{p}_{0|t}) & (\mathbf{A}^\top)^{T-2} \mathbf{B}(\mathbf{p}_{1|t}) & \cdots & \mathbf{B}(\mathbf{p}_{T-1|t}) \end{bmatrix}}_{\mathbf{\Gamma}(\mathbf{P}_t)} \underbrace{\begin{bmatrix} \mathbf{u}_{0|t} \\ \mathbf{u}_{1|t} \\ \vdots \\ \mathbf{u}_{T-1|t} \end{bmatrix}}_{\mathbf{U}_t},$$

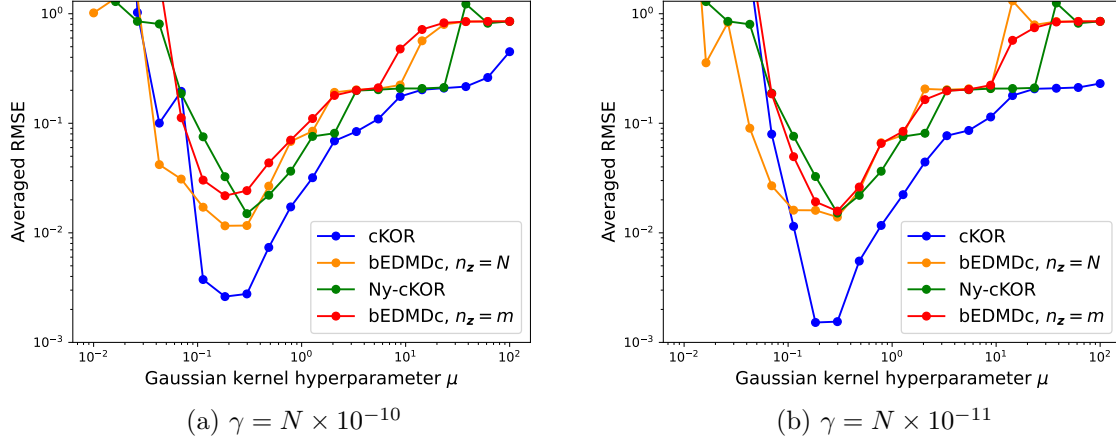


Figure 8: Comparing cKOR, Ny-cKOR and the bEDMDc approaches over values of μ in terms of the averaged prediction RMSE.

The predicted lifted states are used to reconstruct the predicted states over the horizon $\hat{\mathbf{X}}_t$

$$(C.14) \quad \hat{\mathbf{X}}_t = \underbrace{\text{diag}(\mathbf{C}^\top, \mathbf{C}^\top, \dots, \mathbf{C}^\top)}_{\mathbf{C}} \hat{\mathbf{Z}}_t,$$

in order to formulate the constraints and the cost in the original state-space. There are several advantages for remaining in the original state-space as opposed to the lifted state-space: (1) the objectives and constraints are in the original state-space and (2) the number of lifted states is often way larger than the state dimension, i.e. $n_z \gg n_x$. The quadratic program (C.1) and (C.2) can be solved using any QP solver and the first input is applied to the plant after which the process repeats itself in a receding horizon fashion.

Solver. For the numerical implementation of the MPC we rely on the state-of-the-art ForcesPRO solver [27, 97] with freely-available academic licensing.

Appendix D. Supplementary results for the numerical examples.

Hardware. The estimator ablation studies and comparisons were performed on a machine with 2TB of RAM and 4 AMD EPYC 7542 CPUs.

Additional results. Figures 8a and 8b hyperparameter ablation study for even lower levels of regularization $\gamma = N \times 10^{-10}$ and $\gamma = N \times 10^{-11}$. For all these settings, our non-parametric cKOR approach continues to significantly outperform the parametric approaches with its sketched Ny-cKOR version on par or better.

For the control of the Duffing oscillator, Figure 9 illustrates state trajectories over time, corresponding to state plot and input over time figures, i.e Figures 5a and 5b, respectively.

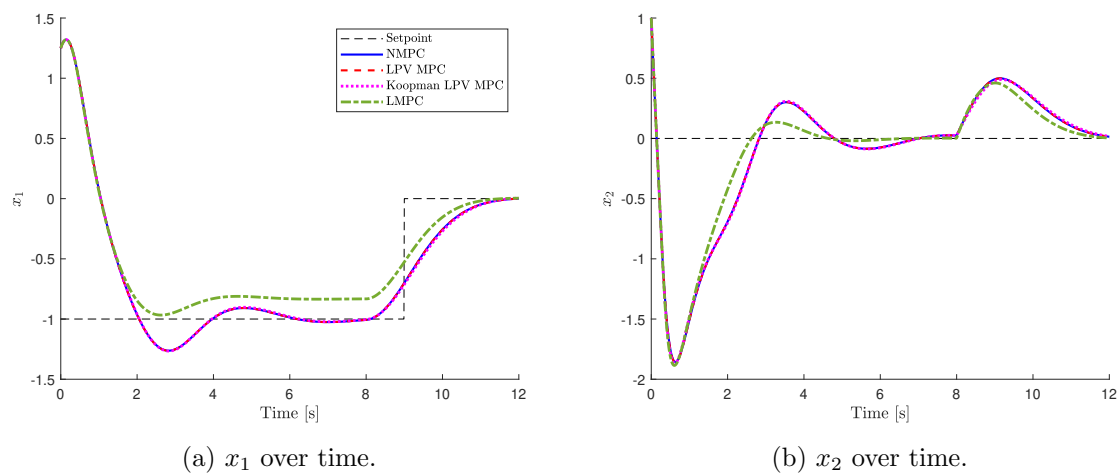


Figure 9: Comparing the resulting trajectories of the MPC approaches.